Precambrian Research 376 (2022) 106695

Contents lists available at ScienceDirect

Precambrian Research

journal homepage: www.elsevier.com/locate/precamres

Anorthosite formation and emplacement coupled with differential tectonic exhumation of ultrahigh-temperature rocks in a Sveconorwegian continental back-arc setting

Trond Slagstad [a,*], Iain H.C. Henderson [a], Nick M.W. Roberts [b], Evgeniy V. Kulakov [c], Morgan Ganerød [a], Christopher L. Kirkland [d], Bjørgunn Dalslåen [e], Robert A. Creaser [f], Nolwenn Coint [a]

[a] Geological Survey of Norway, PO Box 6315 Torgarden, 7491 Trondheim, Norway
[b] Geochronology and Tracers Facility, British Geological Survey, Nottingham NG12 5GG, UK
[c] Centre for Earth Evolution and Dynamics, University of Oslo, PO Box 1028 Blindern, 0316 Oslo, Norway
[d] Centre for Exploration Targeting–Curtin Node, Department of Applied Geology, Western Australian School of Mines, Curtin University, Perth, WA 6102, Australia
[e] Department of Geosciences, University of Oslo, Sem Sælands vei 1, 0371 Oslo, Norway
[f] Dept. Earth & Atmospheric Sciences, University of Alberta, 126 ESB, Edmonton Alberta T6G2R3, Canada

ARTICLE INFO

Keywords:
Sveconorwegian Orogen
Rogaland Anorthosite Province
Bjerkreim–Sokndal layered intrusion
Extensional detachment
Thermo-rheological modeling

ABSTRACT

The tectonic setting and mechanisms and duration of emplacement of Proterozoic massif-type anorthosites and the significance of typically associated ultrahigh-temperature (UHT) host rocks have been debated for decades. This is particularly true of the Rogaland Anorthosite Province (RAP) in the SW Sveconorwegian Orogen. Earlier studies suggest that the RAP was emplaced over 1–3 Myr around 930 Ma towards the end of orogenesis, resulting in an up to 15–20 km-wide contact metamorphic aureole. However, our structural observations show that the RAP is located in the footwall of a 15 km-wide extensional detachment (Rogaland Extensional Detachment, RED), separating the intrusions and their UHT host rocks from weakly metamorphosed rocks in the hanging wall. U–Pb zircon dating of leucosome in extensional pull-aparts associated with the RED yields ages of 950–935 Ma, consistent with Re–Os molybdenite ages from brittle extensional structures in the hanging-wall block that range between 980 and 930 Ma. A metapelite in the immediate vicinity of the RAP yields a 950 Ma U–Pb age of matrix-hosted monazite, and part of the RAP was intruded by the Storgangen norite dike at ca. 950 Ma, providing a minimum age of emplacement. These ages are consistent with Ar–Ar hornblende and biotite ages that show rapid cooling of the footwall before 930 Ma, but slow cooling of the hanging wall. Field and geochronologic data suggest that the RAP formed and was emplaced over a long period of time, up to 100 Myr, with different emplacement mechanisms reflecting an evolving regional stress regime. The distribution of UHT rocks around the RAP reflects differential extensional exhumation between 980 and 930 Ma, not contact metamorphism. The duration and style of orogenic activity and externally (as opposed to gravitationally) driven extension suggest that the RAP formed in a continental back-arc setting.

1. Introduction

The origin of monomineralic massif-type anorthosites is riddled with unresolved questions regarding their source (mantle or crust), tectonic setting (active margin or post-collisional collapse), formation rate (<5 to > 100 Myr), emplacement mechanism (diapirism or migration along active shear zones or conduits), relationship to ultrahigh-temperature metamorphic host rocks, and temporal restriction in the global geologic record to 2.6–0.5 Ga (Ashwal and Bybee, 2017). Few anorthosites have seen more scientific debate of these questions than the Rogaland Anorthosite Province (RAP) in the SW Sveconorwegian Orogen (SNO) of SW Sweden and S Norway. The SNO comprises magmatic, metamorphic, and deformational events between ca. 1140 and 920 Ma at the southwestern margin of Fennoscandia, but the formation of the RAP has never been satisfactorily integrated into this regional tectonic framework.

* Corresponding author.
E-mail address: trond.slagstad@ngu.no (T. Slagstad).

https://doi.org/10.1016/j.precamres.2022.106695
Received 22 October 2021; Received in revised form 26 April 2022; Accepted 26 April 2022
Available online 6 May 2022

The RAP is surrounded by UHT rocks, and existing geochronology and thermal modeling have argued that short-lived (<3 Myr) emplacement of the RAP resulted in an extensive, 15 km-wide UHT contact aureole (Schärer et al., 1996; Westphal et al., 2003). In contrast, other studies have argued that emplacement of the anorthosite may have been protracted (>100 Myr), and that the duration and distribution of UHT metamorphism are incompatible with RAP emplacement alone (Blereau et al., 2019; Bybee et al., 2014; Coint et al., 2015). The tectonic setting of the RAP is also debated, with some arguing for a post-collisional setting (Bingen et al., 2008b; 2021), others for melting of subducted crustal "tongues" (Duchesne et al., 1999), and yet others invoking formation at an active continental margin associated with basaltic underplating (Bybee et al., 2014; Slagstad et al., 2020).

Here, we present new structural observations coupled with precise radiometric age data that provide critical evidence accounting for the contrasting metamorphic histories in the host rocks of the RAP. This new dataset allows thermo-rheological modeling that, when combined with geochronological and petrological evidence, suggest protracted anorthosite emplacement, on the order of 100 Myr. The findings show that the contrasting metamorphic and magmatic features of the SW SNO, compared to other parts of the orogen, reflect late-orogenic exhumation along long-lived ductile extensional detachments, and that different modes of anorthosite emplacement were controlled by a combination of buoyancy and external stresses related to active-margin tectonics.

This study demonstrates a range of discrete tectonic processes and time scales that control the formation and emplacement of such mid- to lower-crustal igneous rock complexes and, importantly, highlights the regional structural control. Thus, while some features may be universal to all massif-type anorthosites, differences in the tectonic evolution, the presence of regional-scale structures, and the thermal state of the crust into which such bodies were emplaced likely led to diversity in the currently observable end-state morphology and lithological relationships of anorthosites and their host rocks.

2. Geological background

2.1. The Sveconorwegian orogeny

The SNO is typically subdivided into five main lithotectonic units (Fig. 1), each with its distinct tectonometamorphic and -magmatic evolution (Slagstad et al., 2020). The SNO was preceded by a long period (ca. 1.3–1.15 Ga) of extensional tectonics at the SW margin of Fennoscandia, with widespread bimodal magmatism and deposition of sedimentary sequences generally inferred to represent a continental back-arc setting (Brewer et al., 2004; Spencer et al., 2014). The onset of Sveconorwegian orogeny is marked by high-pressure metamorphism in the Bamble lithotectonic unit at ca. 1140 Ma. In contrast, neighboring units either experienced continued extension and sedimentation (Telemark) or did not record any activity at all (Idefjorden), suggesting significant separation of the units at that time. A younger, ca. 1100 Ma tectonic event in the Bamble unit coincides with cessation of sedimentation in Telemark and has been interpreted to reflect thrusting of Bamble onto Telemark (Slagstad et al., 2020). From ca. 1080 Ma, the Telemark unit records high-grade metamorphism and voluminous granitic magmatism (Bingen et al., 2008a; Granseth et al., 2020) that lasted until ca. 930 Ma in the SW SNO (Laurent et al., 2018; Slagstad et al., 2018). To the east, the Idefjorden unit records high-pressure metamorphism at ca. 1050 and 1020 Ma (Söderlund et al., 2008), whereas the Eastern Segment records high-pressure, eclogite-facies metamorphism at ca. 990 Ma (Möller et al., 2015). The contrasting metamorphic, magmatic, and depositional histories of different units comprising the SNO led Slagstad et al. (2020) to interpret the Sveconorwegian orogeny as reflecting reamalgamation of the SW margin of Fennoscandia, fragmented during the preceding extensional period. From 990 to ca. 930 Ma, no compressional tectonic activity is recorded; rather, orogen-wide extension is indicated by ca. 980–945 Ma mafic dikes in the eastern orogenic foreland (Söderlund et al., 2005) and 980–930 Ma extensional brittle structures in the SW SNO (this study), lasting until 920–860 Ma and 890 Ma in the eastern and central SNO, respectively (Mulch et al., 2005; Viola et al., 2011). The lack of high-pressure metamorphism and major thrust structures in the central and SW SNO has led most workers to suggest that ca. 1080–930 Ma high-temperature metamorphism and lower-crustal melting reflect ponding of mantle-derived basaltic magmas rather than radiogenic heating following crustal thickening (Bingen et al., 2021; Granseth et al., 2020; Slagstad et al., 2018). To account for the duration of magmatism and metamorphism and considering the absence of significant crustal thickening, Slagstad et al. (2020) suggested that much of the SNO

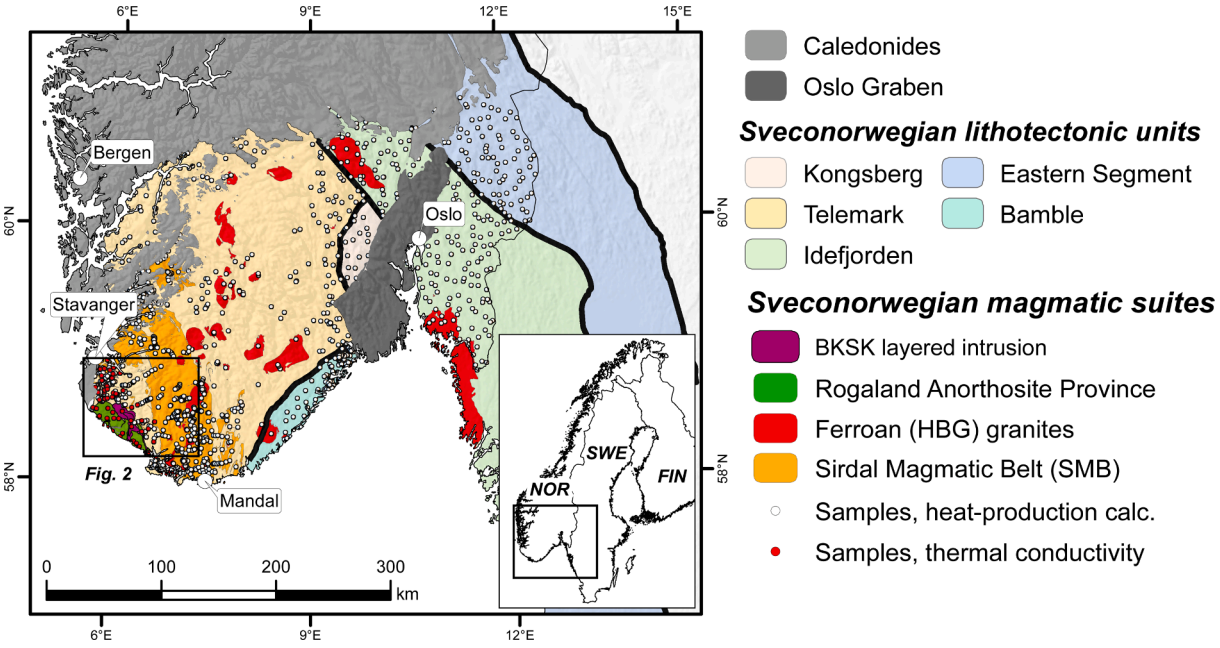

Fig. 1. Geological map draped over a digital elevation model showing the main features of the Sveconorwegian orogen, samples used for heat production calculations and thermal conductivity estimates, and outline of the study area. Thick, black lines indicate tectonic boundaries between the different lithotectonic units.

represents a wide continental back arc, but with little or no *in situ* evidence of the actual arc preserved. Some of the lowermost Caledonian nappes in south-central Norway, generally inferred to represent vestiges of the Baltican continental margin, do, however, contain evidence of an active arc system operating until ca. 940 Ma (Corfu, 2019).

2.2. The SW Sveconorwegian Orogen, high-temperature metamorphism and anorthosite emplacement

Slagstad et al. (2018) subdivided the SW SNO in the Telemark lithotectonic unit by way of a"core area" extending ca. 15 km from the RAP and the spatially associated Bjerkreim–Sokndal layered intrusion (BKSK). Rocks within the core area record apparently continuous (ultra)

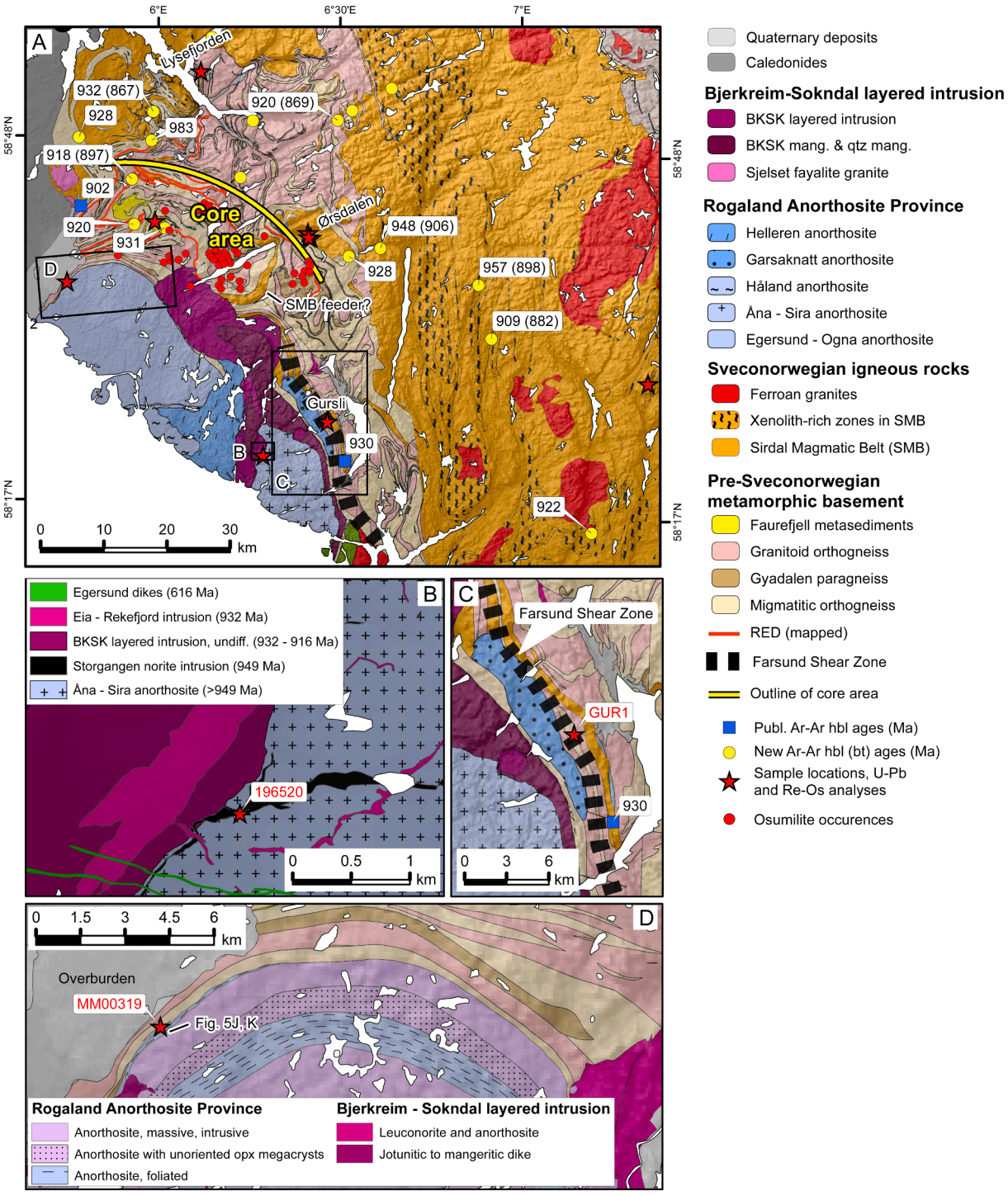

Fig. 2. (A) Geologic map of the main study area in SW Norway. The map is compiled from the 1:250,000-scale Mandal map sheet (Falkum, 1982), the 1:75,000-scale map of the Rogaland Anorthosite Province (Marker et al., 2003), and mapping by the Geological Survey of Norway (NGU) since the early 2000s. The map shows locations of U–Pb samples; Ar–Ar amphibole ages are indicated, with biotite ages (where available) from the same sample in parentheses. (B) Detailed geologic map of the Storgangen intrusion. (C) Detailed geologic map of the Garsaknatt anorthosite in the Farsund Shear Zone. (D) Detailed map of the northern lobe of the Egersund–Ogna anorthosite lobe.

high-grade metamorphism between ca. 1080 and 920 Ma (Fig. 2A). In contrast, rocks outside the core area record high-grade metamorphism between ca. 1070 and 1015 Ma, coeval with emplacement of voluminous granites of the Sirdal Magmatic Belt (SMB, Fig. 2A), followed by emplacement of a suite of younger hornblende-biotite granites (HBG suite). Both suites of granite are largely undeformed and only weakly metamorphosed, thus there is a major, sharp contrast in metamorphic grade and history inside and outside the core area.

The RAP and BKSK are located at the center of the core area and the former consists of four nested lobes of anorthosite with cross-cutting relationships indicating a progression in age from the northern Egersund–Ogna lobe to the southern Åna–Sira lobe (Fig. 2A) (Marker et al., 2003). The Egersund–Ogna lobe is concordant with the tectonic fabric in the gneissic host rocks and Maquil and Duchesne (1984) and Duchesne et al. (1985) argued, based on textural evidence of synmagmatic deformation, for diapiric emplacement. The interpretation of diapiric emplacement was later substantiated by structural and kinematic evidence (Barnichon et al., 1999; Duchesne, 2001), and Charlier et al. (2010) argued that the Egersund–Ogna anorthosite lobe represents a nested diapir. In contrast to the dominant, rounded anorthosite lobes with largely concordant contacts to their host gneisses, the Garsaknatt anorthosite to the SE is elongate and sheet-like and clearly cuts the tectonic fabric in the host rocks (Fig. 2C), indicating a different style of emplacement.

The BKSK is a large layered intrusion consisting from bottom to top of anorthosite, noritic and gabbroic rocks, and mangerite/charnockite and constitutes a through-like intrusion, discordant to both the RAP and high-grade host rocks (Robins et al., 1997). Zircon geochronology has yielded ages of 932–929 Ma for the RAP (Schärer et al., 1996) and 932–916 Ma for the BKSK (Vander Auwera et al., 2011). More recently, however, Bybee et al. (2014) obtained an age of 1040 ± 17 Ma for a high-alumina orthopyroxene megacryst (HAOM) from the Egersund–Ogna lobe and argued for a comagmatic relationship to the plagioclase constituting most of the anorthosite. Rather than short-lived, 2–3 Myr emplacement of the RAP, this work suggested that the RAP and other, similar massif-type anorthosites might have been emplaced over time scales of up to and exceeding 100 Myr.

Samples from the core area yield pressure–temperature (PT) estimates of > 900 °C and > 6 kbar, followed by isothermal decompression to 5–6 kbar (Blereau et al., 2017; Druppel et al., 2013). Although the timing of this metamorphism is typically inferred to reflect emplacement of the RAP and BKSK at 930 Ma (Schärer et al., 1996; Westphal et al., 2003), the observed spread in U–Pb ages provides little geochronological support for such a link, but rather indicates that UHT conditions started much earlier and probably persisted until ca. 930 Ma (Laurent et al., 2018; Slagstad et al., 2018). Drüppel et al. (2013) estimated the timing of peak metamorphism to 1010–1006 Ma. Outside of the core area, the rocks record PT conditions of > 850 °C and > 6 kbar (Blereau et al., 2017), with most age determinations indicating peak metamorphism at ca. 1050–1030 Ma (Slagstad et al., 2018). Decompression to ca. 700 °C and 5.6 kbar is recorded at 955 Ma (Tomkins et al., 2005).

The sharp contrasts in the grade and timing of metamorphism inside and outside the core area suggest that the SW SNO represents different crustal levels juxtaposed during late-orogenic exhumation (Slagstad et al., 2018). However, structural and kinematic evidence of regional, crustal-scale extensional structures that can account for the spatial and temporal distribution of the above geochronological and metamorphic relationships has, until now, been lacking. In this work we use detailed field mapping combined with temporally constrained structural analysis and U–Pb/Re–Os geochronology to determine the geodynamic processes responsible for emplacement and exhumation of the RAP and its UHT host rocks.

3. The Rogaland extensional detachment

Despite mapping of the UHT rocks in SW Norway over several decades, major structures capable of explaining the exhumation of deep-crustal rocks have not been described previously. The current geomorphology of the SW SNO preserves little evidence of the large-scale tectonic structures that may be responsible for the regional-scale distribution and apparent juxtaposition of metamorphic rocks. However, field observations northeast of the RAP reveal a nuanced landscape geometry consistent with the presence of such structures. Fig. 3A shows an atypical landscape scenario for the high-grade gneissic rocks of SW Norway. Most of the landscape is 'symmetric' or 'isotropic'; however, in individual zones a tendency towards topographic 'benching' is observed, with the development of low-angle (20–30°), east-dipping planes (Fig. 3B). Detailed structural analysis of these 'benched' localities reveals a modest but consistent localization of strain over a relatively broad but weak shear fabric (Fig. 3C). Although no conventional mylonitic textures were recognized, we observed modest elongation of both quartz and feldspar grains and commonly sharp tectonic contacts with the adjacent lower-strain gneisses (Fig. 3C). Within these broad zones we also observe truncating fabrics, which we interpret as representing different tectonic fabrics active at different times in the progressive deformation history (Fig. 3D). Deformed clasts within the shear zones are typically symmetric, displaying limited kinematic information, however, the interpreted σ_1 is exclusively vertical suggesting crustal thinning (Fig. 3E).

Symmetric, rootless isoclinal folds are common in the shear fabric (Fig. 3F). These folds have limited kinematic value but are interpreted to represent an early, originally planar version of the shear-zone foliation (for example as shown in Fig. 3H) that has been folded and attenuated and is testament to the protracted deformation sequence in the shear zone. Where shear deformation is observed, porphyroclasts of quartz-rich pegmatites or quartz veins are present and commonly form asymmetric sigma clasts which show consistent down-dip, top-to-E or -NE kinematics (Fig. 3G). In addition, asymmetric rotation of layers within the shear fabric suggests top-to-NE shearing associated with continued extensional deformation (Fig. 3H). Brittle–ductile tension gashes containing granitic/pegmatitic infill and associated with top-to-E or -NE movement along the shear fabric are rare but consistently observed. These tension gashes have typically suffered deformation within the shear zone after their formation and display consistent top-to-E or -NE asymmetries with top-to-E or -NE kinematics (Fig. 3I). As shown in Fig. 3D, the shear fabric is commonly attenuated, boudinaged, and truncated with an asymmetry consistent with the development of outcrop-scale extensional shear bands. These bands display a consistent top-to-E or -NE extensional displacement (Fig. 3J). Mineral stretching lineations, although ubiquitously developed in the shear zone, are relatively weak (Fig. 3K). However, on a regional scale they show a remarkably consistent geometry, plunging NE or E, implying dip-slip or moderately oblique movement on the shear zone. We use U–Pb dating of zircon from leucosomes in tension gash geometries related to the RED to determine the timing of crustal extension (Fig. 3L).

A systematic top-to-E shear sense is identified in a broad zone up to 15 km wide and over a minimum strike length of 40 km in a NNW–SSE-trending ductile shear-zone array consisting of at least six separate shear zones representing a high-temperature, crustal-scale (cf., Andersson et al., 1996) detachment zone (Fig. 4A). We term this shear zone array the *Rogaland Extensional Detachment* (RED). The exact coincidence of this previously unrecognized major extensional structure with the juxtaposition of metamorphic grades strongly supports an interpretation that movement along the extensional detachment was the exhumation mechanism, displacing a weakly metamorphosed, hanging-wall block towards the east, simultaneously exhuming and exposing the juxtaposed high-grade footwall rocks. The interpreted RED outcrop pattern (Fig. 4A) was constructed from a combination of our geometric understanding of the shear-zone localities, the geometry and nature of the underlying bedrock map, and from knowledge of the geometry of major extensional detachment zones worldwide. The red lines on the map represent our interpretation of the complex geometry of the RED.

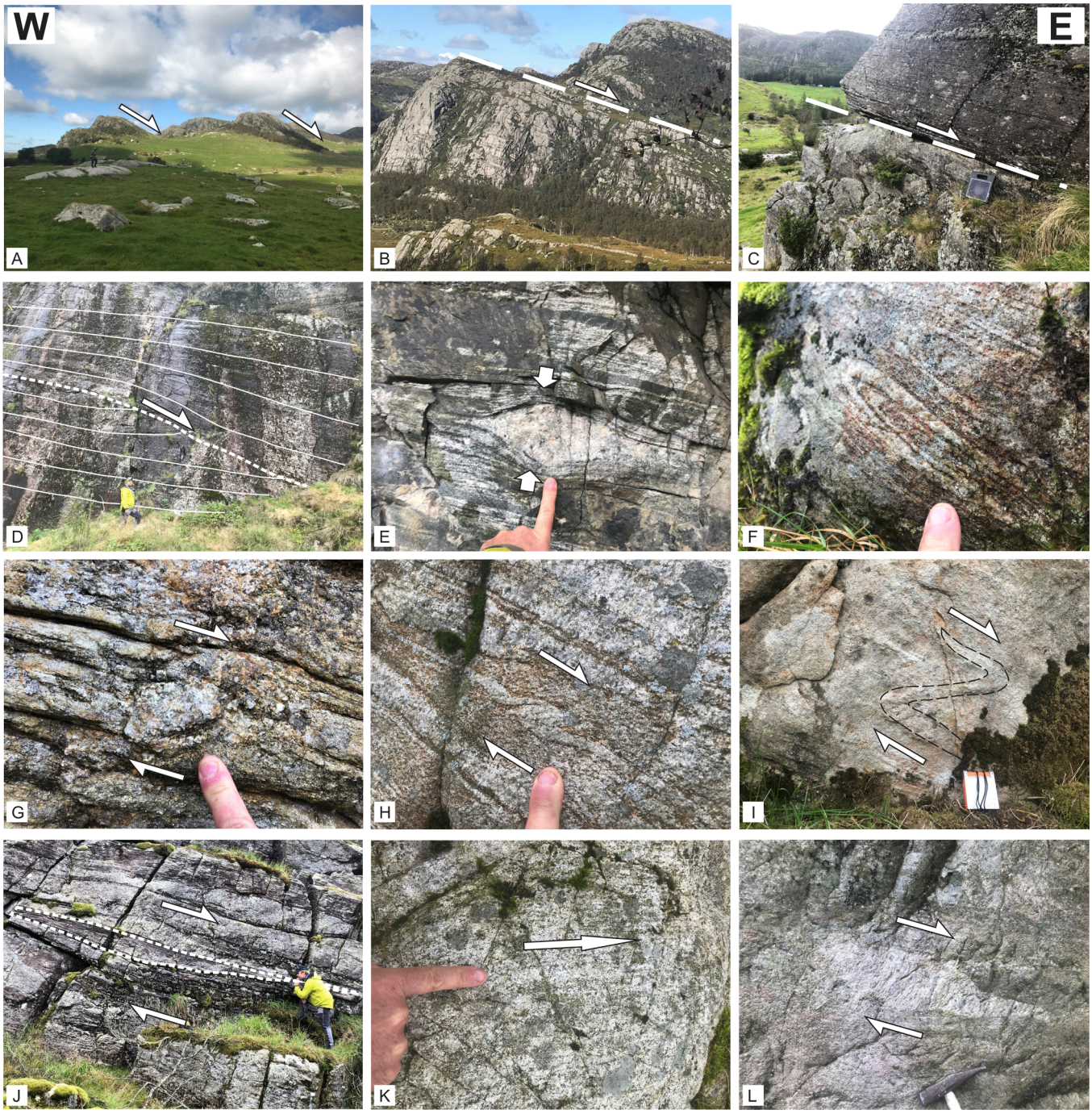

Fig. 3. Key field localities for the identification of geometry and kinematics of the Rogaland Extensional Detachment (RED). All images show west on the left and east on the right. (A) A rather atypical image of the vast swathes of granitic gneiss in SW Rogaland; individual zones show a tendency towards a 'benched' topography where generally meter-wide, but locally up to several-hundred-meter-wide, zones are observed where a generally weak planarity is observed within the granitic gneisses. The foliation dips consistently 20–30° towards the E or NE. (B) Well exposed 'benched' topography consisting of granitic gneiss. Above the line and the kinematic arrow (see other figures) the granitic gneiss is only weakly foliated. (C) Detailed investigation reveals that the 'benching' consists of variably but weakly foliated granitic gneiss with elongated quartz and feldspar grains. The contact to the more weakly foliated granitic gneiss is very sharp in this case, but is typically gradational. We interpret this fabric difference to be a sharp strain gradient between low-strain rock below and high-strain rock above the obvious contact. (D) Two tectonic foliations preserved in a 'benched' zone, suggesting several phases of movement. (E) Porphyroclastic kinematic indicators are rare and commonly symmetric, like the example shown here. However, the symmetric stretching of the clasts suggests a vertical σ_1 and therefore crustal extension. (F) Rootless, symmetric folds formed during protracted deformation of the ductile foliation in the RED. These folds represent an early fabric developed in the shear zone (as seen in 3H, for example) that was folded and attenuated as deformation progressed. (G) Quartz-rich sigma clasts in granitic gneiss showing top-to-E extensional ductile shearing. (H) Clockwise rotation of a quartz-rich layer in granitic gneiss suggesting top-to-E ductile extension. (I) Progressive deformation of a pegmatitic tension gash/vein within the RED along the ductile foliation, demonstrating asymmetric top-to-E kinematics. (J) Protracted deformation and the development of asymmetric boudinage of the shear-zone foliation shows a top-to-E extensional displacement in these deformation zones. (K) Rare, photogenic mineral stretching lineation looking down onto the foliation surface within the RED. The lineation is not particularly well developed but is observed at all shear-zone outcrops and is extremely consistent regionally. (L) Quartz-rich pegmatitic hybrid pull-apart/tension gash on a top-to-E extensional detachment (sample 196516 comes from this tension gash). (For interpretation of the references to colour in this figure legend, the reader is referred to the web version of this article.)

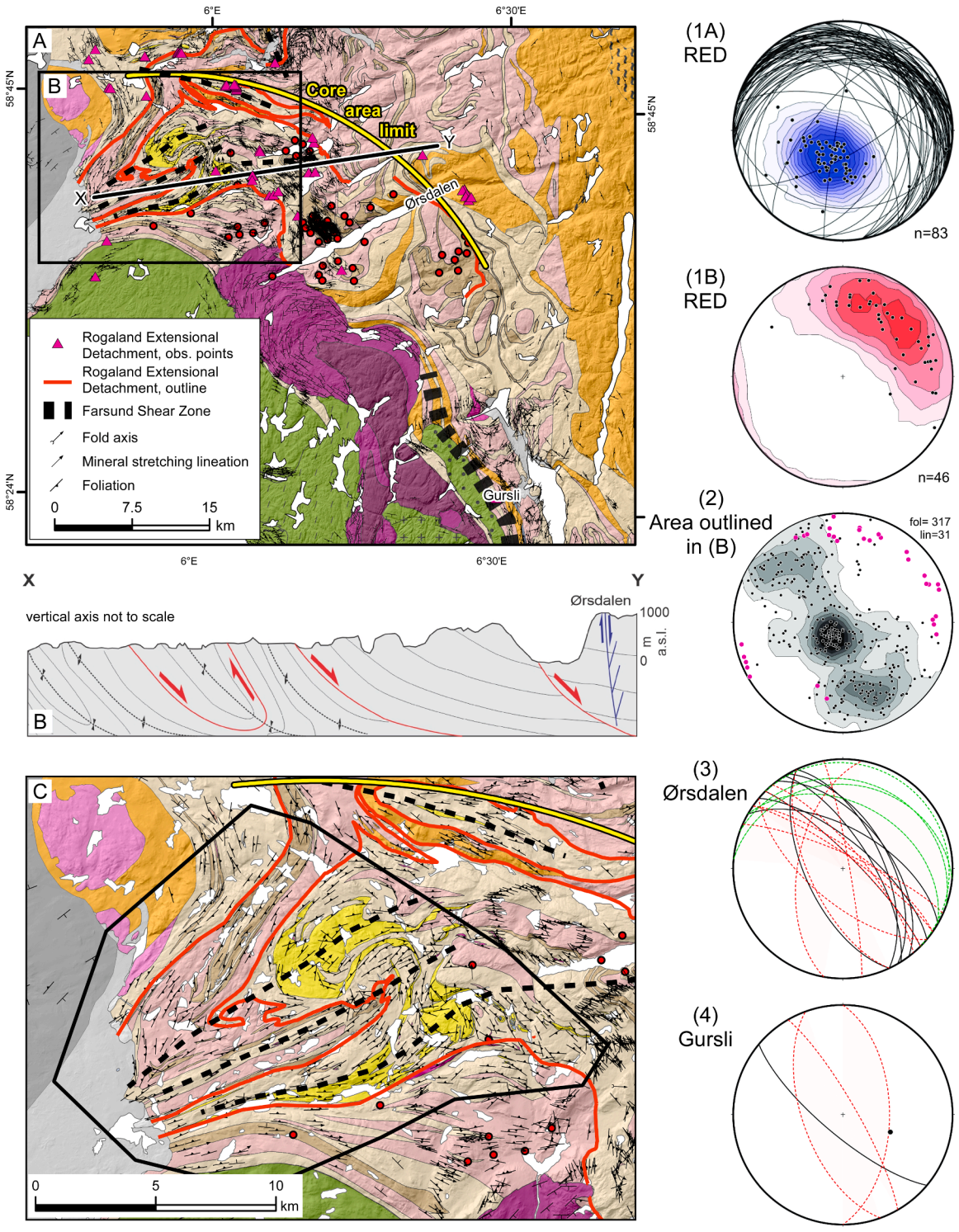

Fig. 4. (A) Tectonic, structural, and kinematic map showing the newly identified Rogaland Extensional Detachment (RED). Pre-existing structural data, both foliations and lineations are in black symbols. Point localities with our new observations of the shear zone are shown with purple triangles and indicate where structural data and observations have been collected. The outline of the interpreted shear zones is shown with a red line and displays a constrictional geometry commonly associated with major ductile detachments. This folding is reflected in stereonets for the foliation (inset 1A) and lineation (inset 1B) of our collected data for whole shear-zone array. The red dots are recorded osumilite occurrences from Tobi et al. (1985) (B) Schematic cross-section showing the folding of the RED and the spatial relationship to the Ørsdalen molybdenite deposit. (C) Detail from 4A showing a selected fold from the interpreted RED showing pre-existing foliation and lineation data. The RED is shown in red and the constrictional folds are dashed black lines. Inset 2 shows poles to foliation and associated contours in grey and the lineation as purple dots. Insets 3 and 4 show stereonets of brittle structural data from two major molybdenite deposits, Ørsdalen and Gursli, respectively. Both show similarly oriented geometries to the RED (NW–SE oriented) and a similar axis of extension (NE–SW). Black great circles are fault planes and breccias and red, dashed great circles are veins. Ørsdalen shows conjugate fault planes but asymmetric vein development, mostly SW dipping. In the Gursli deposit, there is sparse data but shows a similar geometry to Ørsdalen. Both deposits show an extension axis NE–SW, similar to the RED. (For interpretation of the references to colour in this figure legend, the reader is referred to the web version of this article.)

Stereonet data from over 60 shear-zone localities (Fig. 4, inset 1A) show a generally shallowly east-dipping fault plane that is folded on a shallow NE-plunging fold axis. Lineations are generally dip-slip oriented on the RED foliation planes but display a dispersion both to the N and E (Fig. 4, inset 1B), which we interpret to be a result of the folding of the foliation planes. We selected one previously mapped regional-scale fold (outlined by the black polygon in Fig. 4C) in the interpreted RED outcrop pattern for comparison with the focussed RED shear-zone localities. Structural analysis of the pre-existing bedrock mapping data shows a very similar pattern (Fig. 4, inset 2). The foliation displays a generally shallowly NE-dipping geometry but dispersed on a great circle, which suggests folding on NE-plunging axes. In addition, the mineral stretching lineation generally displays a NE plunge, also with dispersion on the NE-plunging fold. Therefore, the RED displays a relatively shallow NE-dipping geometry with a regionally consistent top-to-NE-plunging stretching lineation. Combined with the field kinematics (Fig. 3), this suggests a top-to-NE extensional displacement. The RED is folded regionally on NE-plunging folds that have axes parallel to the transport direction of the extension (Fig. 4B).

We investigated the immediate hanging wall of the RED where, in a broad zone up to 10 km wide, we observed enhanced mineral deposition. Two of the larger molybdenum (±tungsten) deposits in the region, Ørsdalen and Gursli, are located in the hanging- and footwall of the RED, respectively. In both deposits, the molybdenite is almost exclusively deposited in steep quartz veins that are associated with and are commonly secondary structures to relatively thin (up to 30 cm-wide) breccia zones (Fig. 5A), all with strike orientations similar to those observed in the high-grade RED (Fig. 4, insets 3 and 4). These breccia zones are typically localized along amphibolite xenoliths within the granite. The extreme topography in the Ørsdalen valley provides an almost 900 m unique vertical section through different structural levels of this mineralized system. In the upper, relatively cold, more brittle part of the system we observe steep, extensional veins containing only quartz and molybdenite. Fig. 5B shows an extensional quartz vein in the uppermost part of the mineralized system (950 m above sea level), typifying a brittle system with mostly quartz. Fig. 5C shows the lowest part of the mineralized system (50 m above sea level) where the vein geometries are noticeably different and reflect a more flat-lying vein geometry but still within a top-to-E extensional system. Here, the veins are compositionally different, with the presence of wolframite in dominantly pegmatite veins. We interpret these compositional and geometric differences to represent: (1) the deeper part of the extensional detachment system where the extension is manifested in a more shear-related geometry similar to the ductile deformation geometry on the RED, whereas (2) the more brittle and shallower, quartz-rich steep vein systems demonstrate a more purely extensional vein geometry and disintegration of the hanging wall above the RED. Despite the geometrical and compositional differences in the upper and lower parts of the Ørsdalen deposit, the kinematics of the breccia zones and concomitant vein material and mineralization is ubiquitously top-to-NE and extensional. The axis of extension is similar to that observed along the full strike-length of the RED. In the Gursli molybdenum deposit, lying in the footwall of the RED, we observe similarly oriented, steep breccia zones and associated steep extensional quartz veins, which demonstrate top-to-E or -NE extensional kinematics similar to that seen in the Ørsdalen deposit and the RED (Fig. 4, inset 4).

4. Geochronological evidence for long-lived (980–930 Ma) extension, 950 Ma RAP contact metamorphism, and persistent high temperatures in the lower crust

4.1. Samples

The following groups of samples have been collected to address specific questions:

1. In order to determine the timing of deformation on the RED and therefore of regional extension and exhumation along the extensional detachments, we dated:
   a. Zircon U–Pb from pegmatitic leucosome in two extensional pull-aparts (tension gashes) in the footwall to the RED (Fig. 3L, samples 196516, 196517).
   b. Molybdenite Re–Os from four brittle-ductile extensional structures in the hanging wall to the RED in Ørsdalen (Fig. 5A–D; samples ØRS2, STO1, STO3, MJÅ1), as well as from a similar structural site at Gursli, in the inferred footwall to the RED (sample GUR1). A sixth sample was collected at the Flottorp Mo mine ca. 60 km east-northeast of the UHT area (sample FLOT3), where molybdenite is located along steep, brittle extensional structures within SMB granites.
2. Monazite from a metapelite sample taken < 100 m from the RAP was dated in order to constrain the timing of contact metamorphism (sample MM00319).
3. Baddeleyite from the ilmenite-rich Storgangen norite intrusion, that cuts the Åna–Sira anorthosite lobe of the RAP, was dated to provide a minimum age of emplacement (sample 196520).
4. A 2 m-thick andesitic and a 10 cm-thick granitic dike that cut high-grade metamorphic fabrics and SMB granites were dated to constrain the age of melt production in the deeper-orogenic crust following cooling at higher crustal levels (Fig. 4E, F, G, samples BD10.36; ROG132405).
5. New Ar–Ar amphibole and biotite data from samples within and outside the core area provide information on cooling rates during and following the Sveconorwegian orogeny (Fig. 2).

Sample information is summarized in Table 1. Analytical methods and data are presented in Electronic Supplements 1–4.

4.2. Timing of extensional detachment

The two leucosome pull-aparts (samples 196516 and 196517) come from the same outcrop consisting of a quartz-diopside gneiss at lower structural levels in the RED. Samples of the quartz-diopside gneiss taken ca. 4 km away but at the same distance from the RAP, record high-grade metamorphism between ca. 1060 and 940 Ma, with detrital zircon ages ranging between 1.3 and 1.9 Ga (Slagstad et al., 2018). Zircon grains from the two samples are complexly zoned, in some cases with core-rim relationships that correspond to older and younger ages, respectively, although typically the observed core-rim relationships have little age significance. Apart from three, ca. 1.5 Ga grains interpreted to be detrital, most of the analyses range between ca. 1100 Ma and 930 Ma, but with a clear clustering close to the younger end of the age range. The clusters yield weighted average $^{207}Pb/^{206}Pb$ ages of 950 ± 11 Ma (MSWD = 0.31) and 938 ± 11 Ma (MSWD = 0.41) for samples 196516 and 196517, respectively (Fig. 6A–D). These mean ages are similar within uncertainty and interpreted to reflect the age of crystallization of leucosome in the extensional pull-aparts. These ages overlap with the 955 Ma age of decompression recorded at structurally higher levels (Tomkins et al., 2005).

Four molybdenite samples from extensional brittle fractures at Ørsdalen, in the hanging wall to the RED, ca. 19 km from the RAP, yield Re–Os ages ranging from 977 ± 4 to 931 ± 4 Ma (Fig. 8), interpreted to reflect growth and/or recrystallization of molybdenite from hydrothermal fluids passing through the extensional fractures. The range of ages is interpreted to represent repeated brittle faulting during long-lived extension and exhumation, and the formation of a damage zone along the RED, and corresponds to the timing of regional extension determined from dating of mafic dikes and extensional tectonic fabrics east in the orogen (Söderlund et al., 2005; Viola et al., 2011) and inferred from granite petrogenesis in central and western parts of the SNO (Granseth et al., 2020). The younger ages correspond to ductile deformation in the presence of melt at lower structural levels, discussed above. A fifth

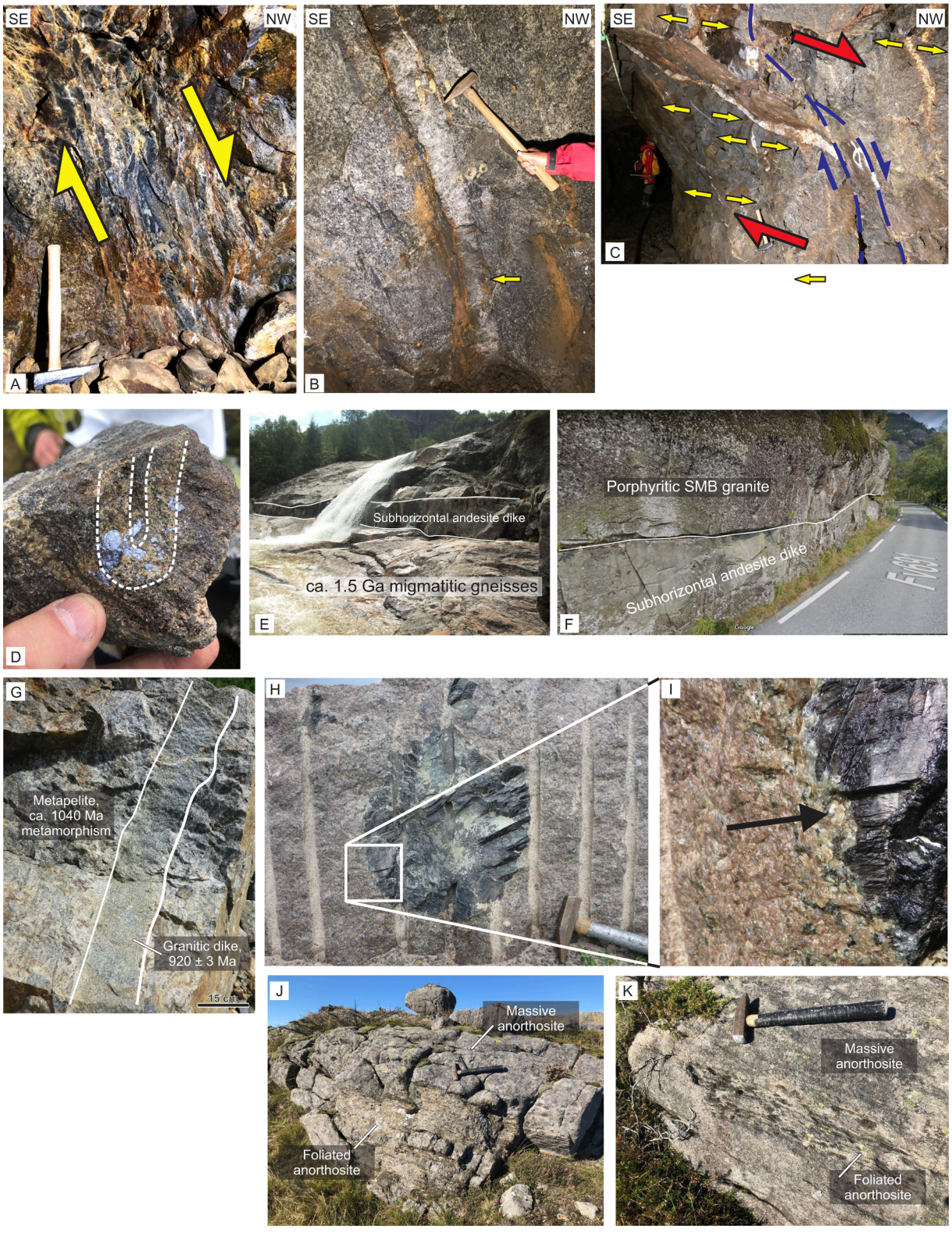

(caption on next page)

Fig. 5. (A) Steeply dipping 30 cm cataclastic zone in the shallowest part of the Ørsdalen deposit (950 m above sea level). The breccia is localized in an amphibolitic xenolith in granite. Kinematics of the rotated clasts suggest a top-to-NE extensional displacement. Quartz veins form as secondary structures spatially associated with the cataclastic zones. (B) Steeply dipping quartz veins with molybdenite in the shallowest part of the Ørsdalen deposit (950 m above sea level) with associated molybdenite deposited in the wall-rock–vein interface (yellow arrow). (C) Shallow-dipping, first-order (red) and second-order (yellow) pegmatitic veins (with molybdenite and tungsten) associated with low-angle extension in the deepest exposed part of the Ørsdalen deposit (50 m above sea level). The low-angle, first-order shear pull-apart shows top-to NE displacement. Second-order tension gashes also show top-to-NE opening associated with the first-order structure. The shallow-dipping structures are cut and displaced by steep brittle faults and veins containing only quartz and molybdenite (blue lines). These are equivalent to the structures in Fig. 5A. (D) Brittle fracture-filling molybdenite cutting older, isoclinally folded leucosome, showing that molybdenite does not date, but clearly post-dates, high-grade metamorphism (cf., Bingen and Stein, 2003). (E, F) Subhorizontal andesitic dikes cutting SMB granites and SNO high-grade rocks (sample BD10.36). (G) Granitic dike (sample ROG132405) cutting high-grade metamorphic fabric in a metapelite near the mouth of Lysefjorden, the latter dated at ca. 1040 Ma. (H, I) High-alumina orthopyroxene megacryst (HAOM) in the Sørskog quarry (Sirevåg), with close-up showing discontinuous lighter-colored zone around the HAOM. (J, K) Strongly foliated anorthosite cut by massive anorthosite at the northern margin of the Egersund–Ogna anorthosite lobe. (For interpretation of the references to colour in this figure legend, the reader is referred to the web version of this article.)

Table 1
Summary of samples and analyses.

Sample	Rock type	Analysis	Longitude	Latitude
MJÅ1	Moly in brittle extensional structure, Ørsdalen	Re–Os moly	6.44157	58.67257
ØSRS2	Moly in brittle extensional structure, Ørsdalen	Re–Os moly	6.43278	58.67941
STO1	Moly in brittle extensional structure, Ørsdalen	Re–Os moly	6.43491	58.67332
STO3	Moly in brittle extensional structure, Ørsdalen	Re–Os moly	6.43491	58.67332
GUR1	Moly in brittle extensional structure, Gursli	Re–Os moly	6.50467	58.41223
FLOT3	Moly in brittle extensional structure, Flottorp	Re–Os moly	7.37027	58.47955
MM00319	Anatectic metapelite, contact to Egersund–Ogna anorthosite lobe	U–Pb mnz	5.78201	58.59586
ROG132405	Granite dike cutting metapelite, Lysefjorden	U–Pb zircon	6.12160	58.90311
196520	Storgangen norite intrusion	U–Pb badd	6.33431	58.36050
196516	Leucosome in tension gash, Nedrebø	U–Pb zircon	6.01409	58.68727
196517	Leucosome in tension gash, Nedrebø	U–Pb zircon	6.01409	58.68727
BD10.36	Horizontal andesite dike, Suldalsosen	U–Pb zircon	6.81076	59.57628
ROG092322	Granitic gneiss	Ar–Ar, bt	6.14764	58.95181
MM02272	Medium-grained hbl–bt granitoid	Ar–Ar, bt	6.26996	58.83553
ROG172	Opx-bearing gneiss	Ar–Ar, hbl, bt	5.94641	58.74551
VAG128025	Megacrystic hbl–bt granite	Ar–Ar, bt	6.54141	58.85548
ROG087	Gray, granodioritic gneiss	Ar–Ar, bt, cpx	6.64719	58.88911
MM01362	Amphibolite	Ar–Ar, hbl, bt	5.99623	58.84272
MM026212	Opx-bearing amphibolite	Ar–Ar, hbl	5.95798	58.68134
MM026213	Opx-bearing migmatitic gneiss	Ar–Ar, hbl	5.79618	58.80158
MM057973	Gray porphyritic granite	Ar–Ar, hbl, bt	6.63159	58.66124
MM02275	Amphibolite	Ar–Ar, hbl, opx	6.04188	58.67795
VAG128027	Medium-grained bt granite	Ar–Ar, hbl, bt	6.50264	58.84115
84397	Strongly foliated porphyritc SMB granite	Ar–Ar, hbl	58.64801	6.54651
BM62	Amphibolite	Ar–Ar, hbl, bt	58.61326	6.90241
BM64	Amphibolite	Ar–Ar, hbl, bt	58.5374	6.94221
BM67	Amphibolite xenolith in SMB	Ar–Ar, hbl	58.26501	7.22769
MM01354	Opx-bearing amphibolite	Ar–Ar, hbl	58.80169	5.99497

Abbreviations: bt–biotite; hbl–hornblende¸cpx–clinopyroxene; opx–orthopyroxene; moly–molybdenite; badd–baddeleyite, mnz–monazite, SMB–Sirdal Magmatic Belt.

Re–Os analysis from Gursli, at a significantly lower structural level than the Ørsdalen samples (Fig. 2), yields an age of 949 Ma, consistent with a progression of brittle deformation to deeper structural levels with increased exhumation and progressive cooling. The sample from Flottorp, ca. 60 km east-northeast of the UHT area, yields an age of 980 Ma, consistent with the earliest recorded extensional structures at Ørsdalen. This suggests that extension was widespread at this time. While the effects of the earlier compressional phase (ca. 1080–1010 Ma) are well documented in the SW SNO from geochronological data discussed above, we have not been able to document compressional structures apart from sparse evidence that the SMB granites in Ørsdalen were assembled during top-to-west thrusting, similar to that observed in central parts of the SMB (Stormoen, 2015). It is possible that the lack of compressional structures in the core area is related to overprinting by long-lived extension.

An earlier Re–Os age of 973 Ma from a migmatite in Ørsdalen was interpreted to date biotite dehydration melting during regional high-grade metamorphism (Bingen and Stein, 2003). Our observations show, however, that the migmatites are found as xenoliths inside weakly metamorphosed, ca. 1050–1030 Ma granites of the Sirdal Magmatic Belt (SMB, Coint et al., 2015) with limited or no deformation and only weakly metamorphosed, and that the molybdenite-bearing brittle fractures cut folded leucosome in the migmatite xenoliths (Fig. 5D). We therefore consider it highly unlikely that molydenite Re–Os ages from Ørsdalen date high-grade metamorphism, as suggested by Bingen and Stein (2003).

4.3. Sustained high temperatures in the lower crust

Several ca. one meter-thick, subhorizontal andesitic dikes occur north in the SW SNO (Fig. 5E, F). The andesitic dikes at Nesflaten, north of the main study area, range in thickness from 0.5 to 2 m and can be traced laterally for several hundred meters; one dike north of Nesflaten is described by Sigmond (1978) to extend for 8 km. The dikes are subhorizontal with sharp contacts to the country rock and intrude both older (ca. 1500 Ma) supracrustal gneisses and younger, undeformed granitic rocks belonging to the SMB. Sample BD10.36 from an andesitic dike yielded prismatic zircon with irregular oscillatory zoning, providing an age of 955 ± 11 Ma (MSWD = 0.19; Fig. 6E), interpreted as the crystallization age of the dike and about 100 Myr younger than the metamorphic fabrics and SMB granites that it cuts.

A decimeter-thick granitic dike cutting ca. 1039 Ma metamorphic fabrics (Slagstad et al., 2018) in a metapelite outside of the core area (Fig. 5G) yielded prismatic to equidimensional, irregular zircon grains that are variably oscillatory and faintly, irregularly zoned. The grains display scattered U–Pb ages as old as 1060 Ma, but with the majority of grains forming a cluster providing a Concordia age of 920 ± 3 Ma (MSWD = 3.4; Fig. 6F), interpreted as the crystallization age of the granitic dike. The excluded analyses (red ellipses) display the same range of ages as the metamorphic zircons from the UHT core area and are interpreted to represent inherited grains from the lower-crustal source of the granitic dike. The age of this dike is therefore > 100 Myr

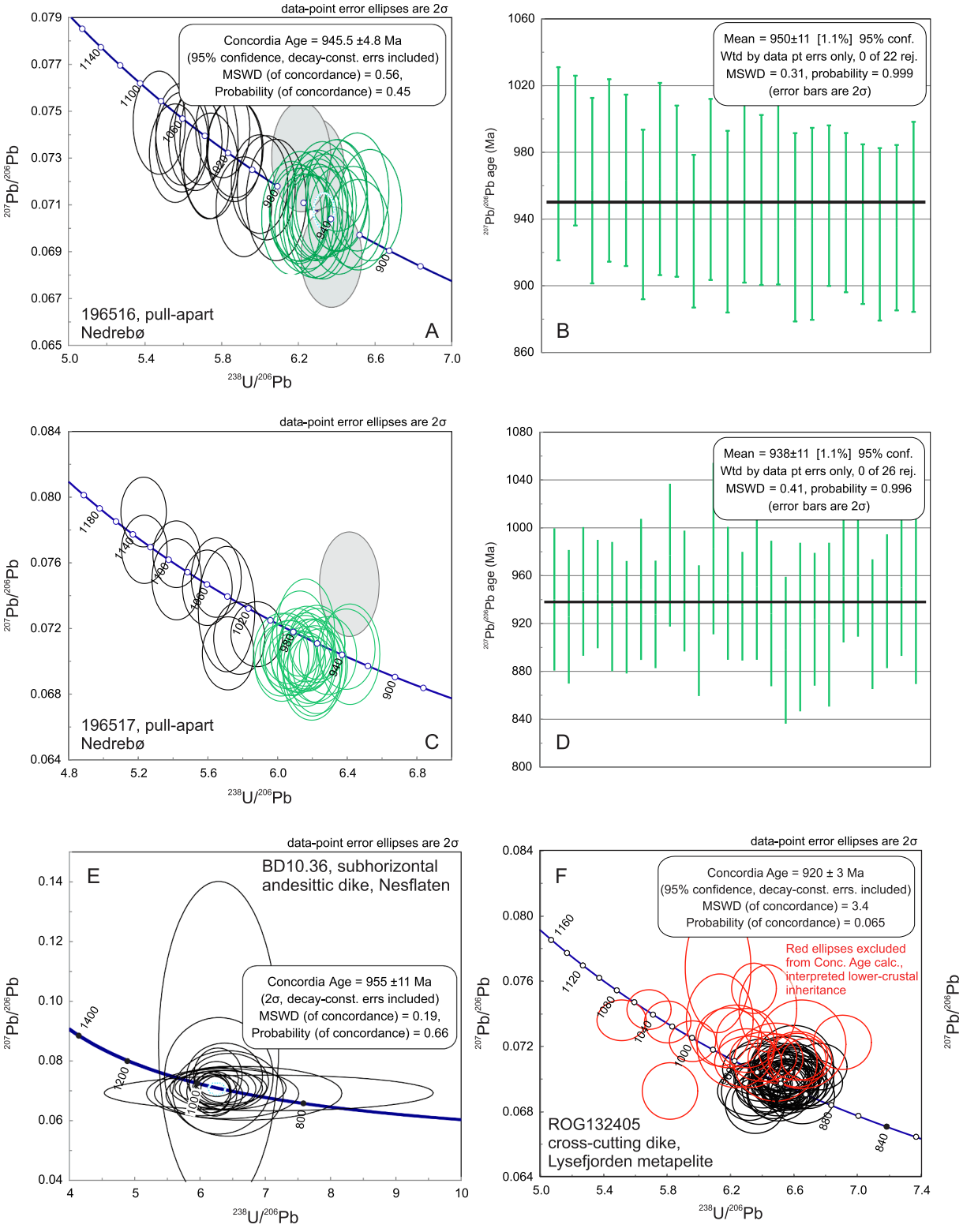

Fig. 6. U–Pb zircon geochronology. (A, B) Tera–Wasserburg plot and $^{207}Pb/^{206}Pb$ weighted mean age, sample 196516, pull-apart tension gash. (C, D) Tera–Wasserburg plot and $^{207}Pb/^{206}Pb$ weighted mean age, sample 196517, pull-apart tension gash. (E) Tera–Wasserburg plot, sample BD10.36, subhorizontal andesitic dike. (F) Tera–Wasserburg plot, sample ROG132405, cross-cutting granitic dike.

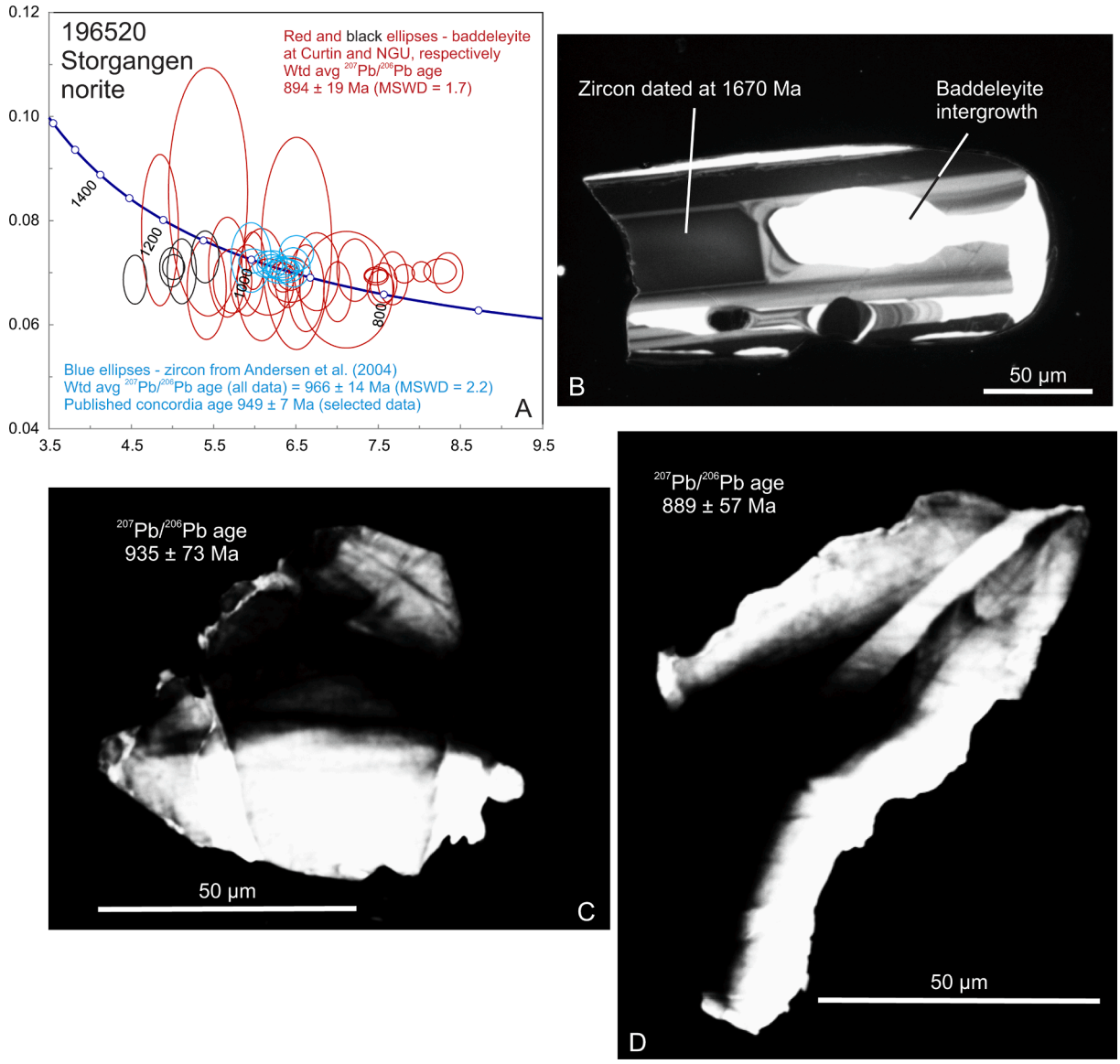

Fig. 7. U–Pb baddeleyite geochronology. (A) Tera–Wasserburg plot and $^{207}Pb/^{206}Pb$ weighted mean baddeleyite age, sample 196520, Storgangen norite. Data from Andersen and Griffin (2004) shown for comparison. CL images showing the (B) zircon–baddeleyite intergrowth and (C, D) heterogeneous baddeleyite crystals.

younger than the fabric it cuts. Both the granitic and andesitic dike indicate that temperatures remained high at deeper crustal levels well outside of the core area in the SW SNO.

4.4. Age of RAP contact (?) metamorphism

Monazite from a UHT metapelite, sampled < 100 m from the contact to the Egersund–Ogna anorthosite of the RAP, was analyzed in order to determine the age of contact metamorphism and, indirectly, the age of RAP emplacement. The sample is from the same locality as the 'proximal sample' of Blereau et al. (2017), that records metamorphic conditions of ca. 950 °C at 5 kbar. In-situ analyses indicate that monazite inclusions in garnet yield weighted mean $^{206}Pb/^{238}U$ ages of 1028 ± 8 (MSWD = 1.5) and 1001 ± 9 Ma (MSWD = 2.4; Fig. 9) for monazite in the garnet cores and rims, respectively, consistent with previous estimates of the timing of regional metamorphism. The matrix monazites, expected to date contact metamorphism, yield a weighted mean $^{206}Pb/^{238}U$ age of 947 ± 10 Ma (MSWD = 1.6; Fig. 9), significantly older than the traditionally inferred 930 Ma age of RAP emplacement (Schärer et al., 1996). A probability plot of the same data yield prominent peaks at 1020 and 955 Ma (Fig. 9B), similar to previously published zircon data (Laurent et al., 2018).

4.5. Minimum age of RAP emplacement, the Storgangen norite intrusion

The Storgangen norite intrudes the Åna–Sira anorthosite (Fig. 2B) and therefore provides a minimum age for the anorthosite. A 949 ± 7 Ma U–Pb zircon crystallization age for the norite intrusion was proposed by Andersen and Griffin (2004), but the implications of this norite age have not been widely appreciated, most likely because their sample was collected from the flotation waste from the mine. However, the age may be of key importance for constraining the timing of emplacement of the RAP. Despite processing several kilos of in-situ norite rock sample, we were unable to extract zircon for U–Pb analysis. However, a few baddeleyite grains and fragments of baddeleyite–zircon intergrowth were recovered. Textural relationships visible under cathodoluminescence (CL) of these grains and fragments (Fig. 7) provide important clues about the relationship between zircon and baddeleyite in this rock. A baddeleyite intergrowth truncates oscillatory zoning in an inherited zircon grain (dated at ca. 1670 Ma), indicating that zircon was replaced by

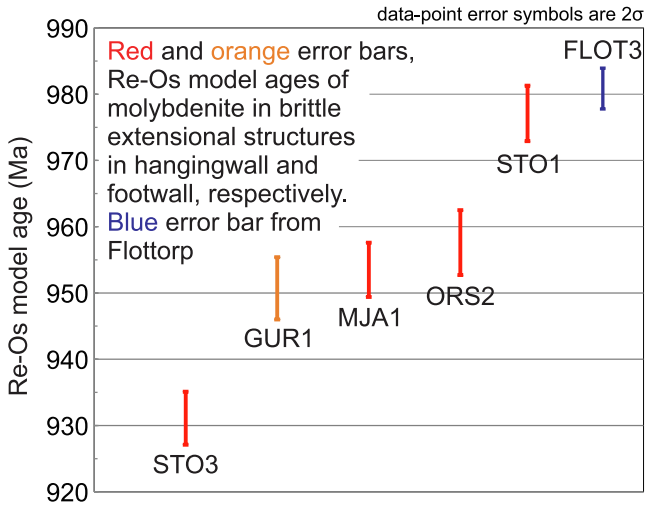

Fig. 8. Re–Os molybdenite model ages with 2σ uncertainties. Red bars from Ørsdalen, orange bar from Gursli, blue bar from Flottorp. (For interpretation of the references to colour in this figure legend, the reader is referred to the web version of this article.)

baddeleyite at some point in the history of this rock (Fig. 7B). Furthermore, other CL images of the dominantly baddeleyite crystals show that they are internally heterogeneous (Fig. 7C, D), similar to crystals formed by alteration related to influx of Ca-rich fluids (Lewerentz et al., 2019). These baddeleyites are, therefore, unlikely to represent primary magmatic crystallization, but rather relate to a later alteration event that involved mobilization of Zr from zircon.

U–Pb baddeleyite and baddeleyite–zircon intergrowth analyses were carried out at Curtin University and NGU. At NGU, the analytical protocol was similar to that of zircon, i.e., using GJ zircon as the primary reference material, whereas at Curtin University Phalaborwa baddeleyite was used. It is well known that baddeleyite analyses are sensitive to U–Pb elemental fractionation in secondary ionization mass spectrometry due to crystal orientation effects and dissimilar ablation response to the reference material (e.g., Wohlgemuth-Ueberwasser et al., 2018). Laser analyses are typically less sensitive to crystal orientation effects; however, the intimate nature of the intergrowths and the heterogeneous ablation signal (as evident especially in Th) highlight the complexity of matrix matching this material. Ablation integration periods were chosen on the most homogeneous part of the ablation signal. Given the textural evidence suggesting that the dated material represents intergrowth of baddeleyite and zircon, we interpret the spread in $^{238}U/^{206}Pb$ ratios to reflect matrix mismatching and hence this ratio has little chronometric resolution for this material. Thirty-three analyses of the most pristine baddeleyite yield a weighted average $^{207}Pb/^{206}Pb$ age of 894 ± 19 Ma (MSWD = 1.7). This age is within error of the youngest phases of the BKSK (Vander Auwera et al., 2011) and considering that both the Storgangen intrusion and its host rock show signs of deformation related to emplacement of the BKSK (Schiellerup, 2001), we interpret the baddeleyite to have grown as a result of fluid activity linked to intrusion and deformation at this time.

While these baddeleyite $^{207}Pb/^{206}Pb$ data only provide a minimum age for the Storgangen intrusion, we note that several of the crystals dated by Andersen and Griffin (2004) display bright, irregular patches in backscatter electron images, consistent with the presence of baddeleyite intergrowths in their zircon. This characteristic textural relationship of the crystal cargo of the Storgangen intrusion supports the interpretation that the material dated by Andersen and Griffin (2004) is indeed locally derived. Hence, their 949 ± 7 Ma age for the zircon component provides the best estimate of the primary magmatic crystallization of the Storgangen intrusion. This ca. 950 Ma zircon age provides a minimum age for emplacement of the Åna–Sira anorthosite lobe – notably the youngest lobe in the RAP.

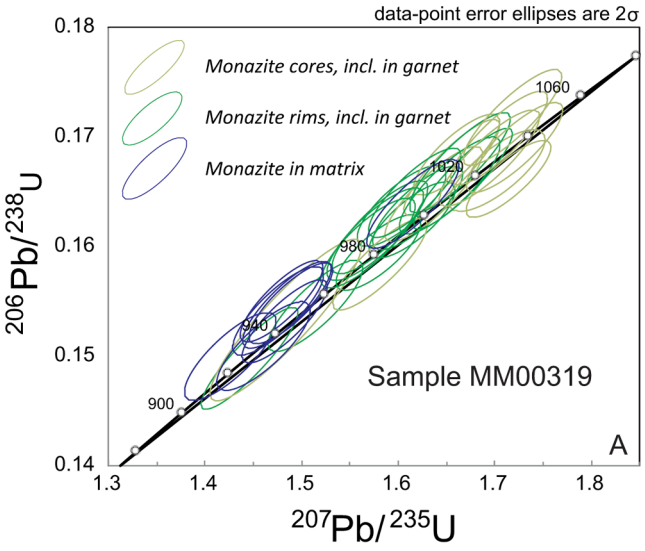

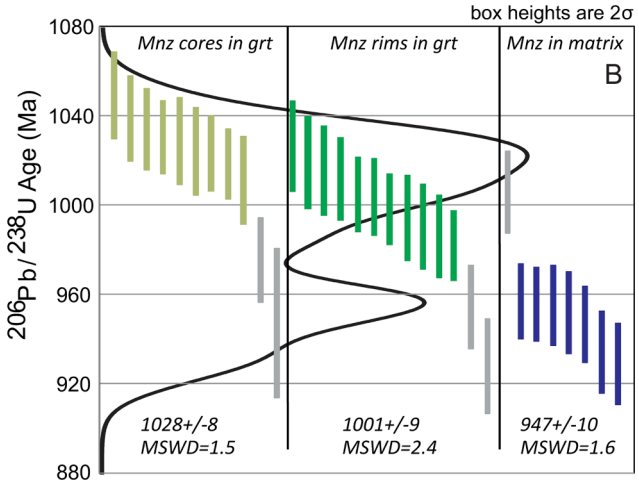

Fig. 9. U–Pb monazite data from sample MM00319. The data have been subdivided texturally into monazite inclusions in garnet cores and rims, as well as monazite in the matrix. Abbreviations: Mnz – monazite; grt – garnet; incl – inclusion.

4.6. Ar–Ar amphibole and biotite ages constrain the timing and rate of cooling

Sixteen samples within and outside of the core area were collected for Ar–Ar geochronology in order to constrain the cooling history of the SW SNO. The samples include amphibolites, amphibolite- to granulite-facies granitoid gneisses, and granites of the SMB. New and existing Ar–Ar amphibole ages range between 983 and 902 Ma (Fig. 2A; Bingen et al., 1998; this study), but with the majority (10 of 15) between 932 and 918 Ma (Fig. 2). There is no apparent difference in age with distance from the RAP. Ar–Ar biotite ages, like amphibole, show no difference across the extensional detachment, ranging from 906 to 867 Ma. The difference between Ar–Ar amphibole and biotite ages for the same sample ranges from 22 to 65 Myr, with an average of 45 Myr.

5. Discussion

5.1. Timing and distribution of high-grade metamorphic rocks in SW SNO

The (U)HT rocks in the SW SNO were traditionally inferred to

represent the high end of a gradational metamorphic spectrum, from (upper) amphibolite facies in central parts of the SNO to granulite facies in the SW, thus accounting for a westward change from hydrous to more anhydrous magmatism across an orthopyroxene-in isograd (Vander Auwera et al., 2011). The UHT rocks, confined to an area within 10–15 km of the RAP, were interpreted to reflect contact metamorphism during short-lived (ca. 3 Myr) emplacement of the RAP and BKSK at 932–929 Ma (Westphal et al., 2003). Coint et al. (2015), however, showed that there is no such gradual, regional transition and that the 'orthopyroxene-in isograd' is, in fact, an intrusive contact between granulite-facies rocks and the SMB granites, with the only amphibolite-facies rocks east of the 'isograd' occurring as screens and xenoliths in the granites. Similarly, the previously interpreted osumilite-in contact-metamorphic isograd around the RAP was shown by Blereau et al. (2019) to be related to much older (ca. 1070 Ma) regional metamorphism. Nevertheless, the nearly symmetric distribution of osumilite (and pigeonite) around the RAP and BKSK (Tobi et al., 1985) (Fig. 2A) does seem to suggest some sort of relationship. This relationship can now be understood within the structural context of the RED, which coincides with the osumilite and pigeonite-in isograds. In this case, the isograds simply represent tectonic juxtaposition of different crustal levels, consistent with the onset of high-T metamorphism and crustal melting at ca. 1070 Ma, followed by differential exhumation along the RED, giving the impression of a wide contact aureole.

The geologic history of the SW SNO became even more confounding when the high-Al orthopyroxene megacrysts (HAOMs) in the RAP yielded a Sm–Nd isochron age of ca. 1040 Ma (Bybee et al., 2014), i.e., >100 Myr older than the accepted age of the anorthosite. The HAOMs have compositions indicative of crystallization at pressures of 11–13 kbar (Charlier et al., 2010; Longhi et al., 1993), thus both age and depth suggest that emplacement of the RAP could not have caused UHT contact metamorphism of its host rock at ca. 6 kbar at 930 Ma, consistent with the extended duration of (U)HT metamorphism. The ca. 950 Ma age of the Storgangen norite intrusion (Andersen and Griffin, 2004; this study), cutting the RAP, also suggests emplacement well before the widely accepted age of 930 Ma. This interpretation is supported by monazite age data presented here for a metapelite sample taken<100 m from the RAP that records a range of metamorphic ages from 1028 to 947 Ma, but with no indication of a high-grade metamorphic overprint at 930 Ma. Ti-in-zircon temperatures from UHT rocks in the footwall of the RED show an increase from ca. 760 °C to 820 °C at 970 Ma (Slagstad et al., 2018), consistent with emplacement of at least part of the RAP significantly earlier than 930 Ma and, lastly, Ar–Ar amphibole data show that the UHT rocks close to the RAP had cooled significantly by ca. 930 Ma, inconsistent with a major thermal pulse at this time.

Until the discovery of the RED, the distribution of metamorphic and non-metamorphic rocks required impossibly large lateral temperature gradients in the deep orogenic crust and although zircon from the anorthosites undoubtedly yield ca. 930 Ma ages, short-lived emplacement of the RAP and BKSK at ca. 930 Ma, with a large contact-metamorphic overprint, is inconsistent with the currently available data. The newly identified RED, a 15 km-wide zone of diffuse but broad and consistent high-temperature ductile deformation on which the northeastern hanging-wall block was displaced orthogonally to the NE, accounts for the spatial and temporal distribution of metamorphism in the SW SNO and removes the need for large lateral thermal gradients in the deep orogenic crust. At approximately 980 Ma, the crust began to extend in the SW SNO (Mulch et al., 2005; Scheiber et al., 2015; Slagstad et al., 2020; Viola et al., 2011). This extension was focused on the NW–SE-striking, relatively shallowly E-dipping RED, exhuming the high-grade rocks in the footwall and contributing to upper crustal emplacement of the RAP, discussed below. In addition, the presence of steeply dipping, brittle cataclastic zones and fractures in the hanging wall, the kinematics and timing of which are similar to that of the RED, shows that these are secondary structures related to movement on the RED and most likely represent the at least partial disintegration of the hanging-wall block.

5.2. *Varied mechanisms for long-lived anorthosite emplacement*

Crustal heating during orogeny results either from crustal thickening and internal radiogenic heat production and/or heat supplied by mantle-derived melts ponding at the Moho or intruding the overlying orogenic crust. The average heat production in the western and central SNO from 1689 whole-rock geochemical analyses (Fig. 1 and Electronic Supplement 5) is 1.81 μW/m^3, whereas weighting the data by area of the sampled geological units (50,000 map scale, see Slagstad, 2008 for procedure) yields a slightly higher average heat production of 2.16 μW/m^3. Such values can only account for temperatures in the lower crust (40 km depth) of up to ca. 600 °C (Clark et al., 2011), which is clearly at odds with the PT conditions in the SW SNO, particularly considering a maximum crustal thickness on the order of 40–45 km based on the HAOM data. These observations suggest that heat was primarily added from below in the form of mafic magma and that this process was long

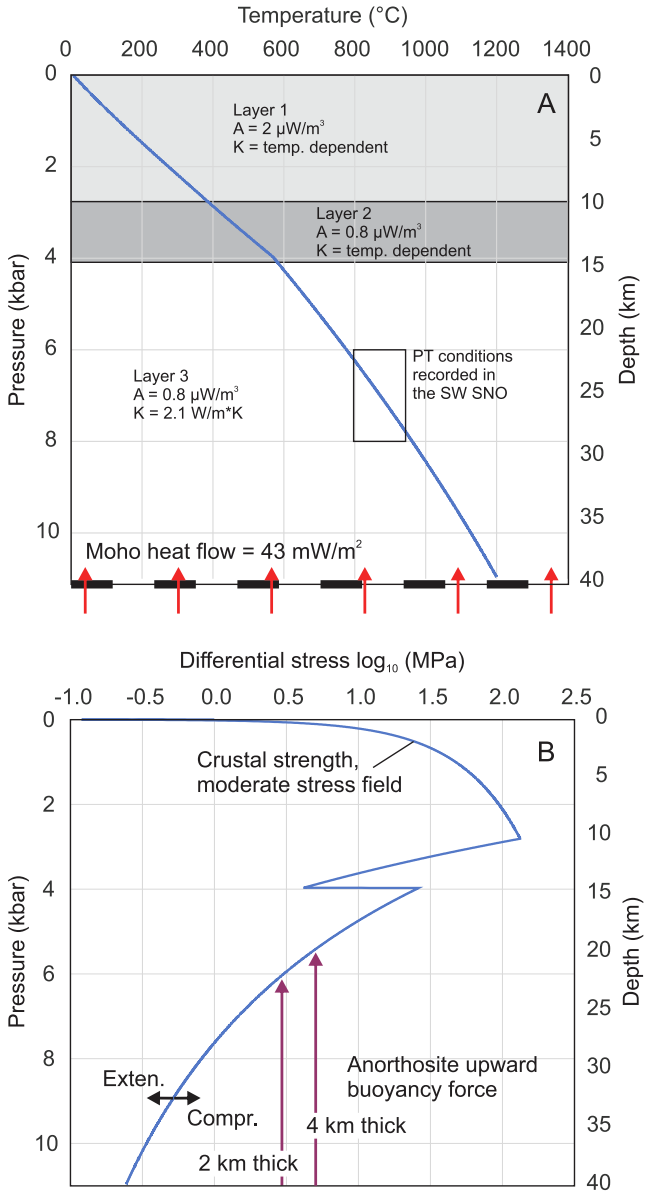

Fig. 10. Thermo-rheological modeling with relevance to anorthosite emplacement. See text for details. The thermal model reproduces the observed PT conditions in SW SNO (box).

Table 2
Thermal and rheological parameters used in thermo-rheological modeling.

Thermal parameters		Rheological parameters[2]	
Temperature at surface (°C):	5	Gas constant (R)	8.314
Heat flow across Moho (mW/m^2):	43	Strain rate (epsilon)	1.00E-15
		Density upper and middle crust	2700
		Density lower crust	2850
Layer 1 Upper crust		g	9.81
Top of layer (km)	0	Pore fluid factor (λ)	0.37
Base of layer (km)	10	Numerical factor (alpha)	0.75
Heat production (μW/m^3):	2	Pre-exponential stress constant (MPa^{-n}/s)	A
Conductivity (W/m*K)	Temp. dep.[1]	Power-law exponent	n
		Activation energy (kJ/mol)	E
Layer 2 Middle crust			
Top of layer (km)	10	Upper and middle crust (quartz diorite)	
Base of layer (km)	15	A	1.26E-03
Heat production (μW/m^3):	0.8	n	2.4
Conductivity (W/m*K)	Temp. dep.[1]	E	219
Layer 3 Lower crust		Lower crust (undried diabase)	
Top of layer (km)	15	A (MPa^{-n} s^{-1})	2.00E-04
Base of layer (km)	40	n	3.4
Heat production (μW/m^3):	0.8	E	260
Conductivity (W/m*K)	2.1		

[1] Temperature-dependent thermal conductivity K(T) of upper and middle crust, with K at surface temperature (5C) of 2.8, calculated from: K(T) = A + B/(350 + T(z), where A = 0.75 and B = 705.

[2] Ductile and brittle strength calculated following Afonso and Ranalli (2004) using rheological parameters from Slagstad (2006).

lived, probably spanning most of the 1080–930 Ma time interval (Bingen et al., 2021; Granseth et al., 2020; 2021; Slagstad et al., 2018).

In order to address the juxtaposition of isograds in the SW SNO and possible emplacement mechanisms for the RAP, we calculated a simple, 1D crustal thermal profile (Fig. 10A). The thermal parameters used are presented in Table 2, and include a temperature-dependent thermal conductivity in the upper 15 km of the crust (2.8 W/m*K at the surface (5 °C) following Zoth and Hänel, 1988). The thermal conductivity is constrained by 62 samples from the SW SNO (Fig. 1; Electronic Supplement 5). Between 15 and 40 km depth, a constant conductivity of 2.1 W/m*K is assumed as conductivities tend to converge at temperatures > 400 °C (Clauser and Huenges, 1995). Heat production was set at 2 μW/m^3 in the upper 10 km (similar to surface values) and 0.8 μW/m^3 at depths of 10–40 km. With a 'Shield-like' basal heat flow of 15 mW/m^2 (Jaupart and Mareschal, 1999), these values yield a surface heat flow of 59 mW/m^2, which is consistent with the observed present-day heat flow in the SNO (Slagstad et al., 2009). In the SNO model, the basal heat flow is set to 43 mW/m^2, which corresponds to a Moho temperature (at 40 km depth, constrained by the HAOM data) of 1200 °C, similar to the estimated liquidus temperature of the parental melt to the anorthosite (Westphal et al., 2003). This model yields temperatures between ca. 800 and 1000 °C at pressures of 6–8 kbar (Fig. 10A), consistent with PT estimates from SW SNO, and a surface heat flow of nearly 90 mW/m^2. The extreme lower-crustal temperatures (1200 °C at 40 km depth) would be alleviated by assuming convective heat transfer in the lower crust or a thinner crust, both of which are possible given the available data. By assigning appropriate rheological parameters and densities to the different crustal segments (see Table 2), the thermal model also allows us to calculate the strength of the crust (given a moderate stress regime) and compare with the buoyancy force of an anorthosite body of a certain thickness (Fig. 10B). The rheological parameters are the same as those previously used by Slagstad (2006) in the central SNO. Magnetic data suggest that the anorthosite is ca. 2 km thick (Maystrenko et al., 2017), whereas gravimetric data suggest a thickness of 4 km (Smithson and Ramberg, 1979), but the thickness lost to erosion is unconstrained. Assuming thicknesses of 2 and 4 km, with a density contrast of 150 kg/m^3, the modeling shows that in a moderate external stress field, the anorthosite can rise buoyantly to depths corresponding to 5–6 kbar, which is similar to petrologically based estimates (Charlier et al., 2010) and the modeling of Barnichon et al. (1999) and Mukherjee et al. (2020). Barnichon et al. (1999) estimated that this process would take on the order of 2.5 Myr, however, a compressional stress field, as documented for the SNO in the period 1070–1010 Ma, would have prevented the anorthosite from rising to these depths by pure buoyancy – at least until the regional stress field changed to moderate or extensional. Data from mafic dikes in the SNO foreland show that extension had started there by 970 Ma (Söderlund et al., 2005), and an increase in temperature to form granitic melts from more refractory sources from ca. 990 Ma onwards suggests increased and more widespread influx of basaltic melts to the base of the crust at this time (Granseth et al., 2020). The increased basaltic influx was interpreted to reflect a change from a compressional to an extensional stress regime at this time, consistent with the kinematics, structural geometries, and geochronological data presented here, and could have allowed the anorthosite lobes to rise to shallower levels, in keeping with their polybaric evolution (Charlier et al., 2010).

Although emplacement of the RAP and BKSK is typically inferred to have happened over only 2–3 Myr at ca. 930 Ma, the available geochronological data, geological/structural observations, and thermo-rheological modeling discussed above suggest a significantly longer-lived process. Field relationships also suggest a comparatively long-lived event; for example, the oldest anorthosite bodies had time to cool sufficiently to acquire tectonic fabrics before being cut by younger, undeformed anorthosites (Marker et al., 2003). The oldest anorthosite body, the Egersund–Ogna lobe, shows complete parallelism with its UHT host rocks, compatible with emplacement by diapirism (Fig. 11A), previously suggested based on petrological, structural, and kinematic evidence (Barnichon et al., 1999; Duchesne, 2001; Duchesne et al., 1985; Maquil and Duchesne, 1984). The northern part of the deformed Egersund–Ogna lobe and its immediate host rock is, however, cut by a sheet of undeformed anorthosite (Fig. 4J, K; Blereau et al., 2017; Marker et al., 2003) which must be younger, intruding a previously up to 3 km-wide margin of strongly foliated anorthosite and possibly accounting for zircon diffusion modeling suggesting a short-lived thermal pulse there (Blereau et al., in press).

In contrast, the elongate, NNW–SSE-oriented Garsaknatt anorthosite body clearly cuts the high-grade fabrics of its host rocks (Marker et al., 2003) and shows no signs of diapirism (Fig. 2C). Emplacement of the Garsaknatt body could be related to migration along the continuation of the RED (Fig. 11B), possibly merging into the extensional Farsund Shear Zone (Fig. 2C, Bolle et al., 2010). Directly dating the crystallization of the Garsaknatt anorthosite remains an important test of this model.

We posit a long-lived emplacement history of the RAP, possibly in excess of 100 Myr, based on geochronology, thermal and buoyancy modeling, and field relationships, and argue that the notion of emplacement of the RAP and BKSK on time scales of 2–3 Myr is highly unlikely. Our interpretation is consistent with previous interpretations that long-lived magmatism and high-grade metamorphism in the SW SNO was largely driven by near-continuous emplacement of mantle-derived mafic magma (Granseth et al., 2020; 2021; Slagstad et al., 2018) – there is no reason to believe that anorthosite magma would only have formed once during this process. These features also suggest that the long-lived extension along the RED was not only integral in exhuming the UHT rocks, but also allowed anorthosite magmas to rise buoyantly and/or along active structures to mid-crustal levels and that this exhumation was driven by crustal thinning along a NW–SE-striking array of wide ductile detachments with top-to-E or -NE displacement.

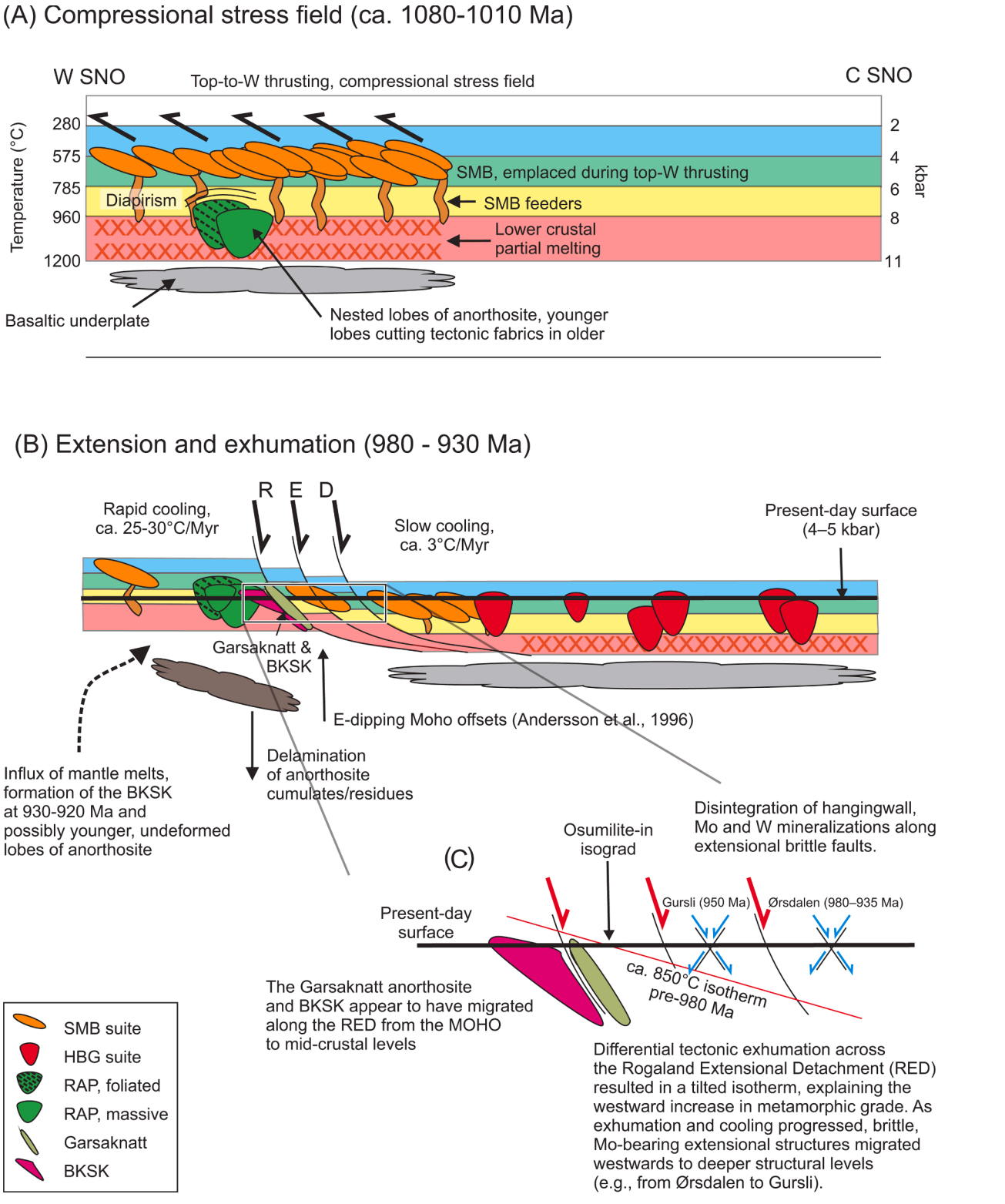

(caption on next page)

Fig. 11. Simplified tectonic model of SW SNO, subdivided into an early compressional phase (ca. 1080–1010 Ma) and a later extensional phase (ca. 980–930 Ma). (A) During compression, mantle-derived basaltic magmas provide heat and material to the lower crust. Partial melting of the lower crust and variable mixing with the basaltic melts generate the SMB granites. Models for anorthosite petrogenesis either suggest fractionation from the mantle-derived basaltic melts or large degrees of partial melting of the lower crust to form the basaltic melt. We do not present new data either way, but the thermo-rheological modeling suggests that the anorthosite bodies could rise diapirically into the lower-crustal UHT rocks, although not to their current level of exposure (at most 6–7 kbar). (B) During extension, diapiric rise to shallower crustal levels (ca. 5 kbar) would be possible, but progressively less efficient as exhumation and cooling of the anorthosite host rocks took place. Continued flux of mantle-derived basaltic melts means that anorthosite could have been produced continuously, but with a greater structural control on anorthosite emplacement along discrete shear zones (e.g., Garsaknatt). As discussed in the text, flow or percolation of younger anorthosite through older bodies may also account for the 930 Ma ages from the RAP. This continued flux of anorthosite could be responsible for the comparatively young zircon ages obtained from the RAP. An implication of this model is that the BKSK and RAP are genetically unrelated. The BKSK formed relatively late in the orogenic history and has typically been ascribed to a delamination event. Considering the apparent lack of crustal thickening, we propose that the dense cumulates following anorthosite formation may have delaminated and triggered one last, short-lived magmatic event forming the BKSK, prior to the onset of widespread cooling and tectonic quiescence. The spatial and temporal coincidence of the RED and BKSK suggest that migration and emplacement of the latter was structurally controlled. (C) Zoom-in on the RED and its immediate foot- and hanging wall. Disintegration of the hanging wall resulted in brittle extensional structures that accommodated deposition of Mo between 980 and 935 Ma (Ørsdalen). Brittle deformation progressed to deeper structural levels during exhumation and cooling of the footwall (Gursli). Differential exhumation resulted in a tilted isotherm, which accounts for the distribution of HT/UHT rocks in the SW SNO. (For interpretation of the references to colour in this figure legend, the reader is referred to the web version of this article.)

The tectonic significance of this long-lived evolution is discussed further below.

The generally accepted age of 930 Ma for the RAP stems from U–Pb analysis of zircon "extracted from orthopyroxene megacrysts" (Schärer et al., 1996). However, given the much older, ca. 1040 Ma age of the HAOM themselves, exactly how the zircons found their way into these crystals remains elusive. We have rigorously searched for zircon in polished HAOM slabs via repeated polishing to expose deeper parts of the slabs. However, no zircon was found. Instead, the dominant Zr-bearing phase identified was baddeleyite, forming small grains within ilmenite exsolutions. We suggest that the 930 Ma zircons with well-developed, igneous sector zoning (Slagstad et al., 2018) did not form inside the HAOMs. Field observations of the HAOMs reveals that many of them are partially rimmed by cm-thick, light-colored anorthosite (Fig. 5H, I). The lighter rims do not appear to represent post-magmatic bleaching, which would be expected to be more homogeneously developed around the HAOMs. A testable hypothesis is that the light rims represent evolved melt that was trapped in pressure shadows around the HAOMs, possibly as the melt was migrating from deeper crustal levels. A similar feature has been observed in the mafic–ultramafic Lower Zone of the Bushveld Complex, where Karykowski and Maier (2017) argued that dating interstitial zircon from cumulates is unlikely to record the timing of emplacement (see also Latypov and Chistyakova, 2021).

The Ar–Ar amphibole data show that cooling through the closure temperature of Ar in amphibole (taken here as 550 °C) took place before 930–920 Ma in most samples. For samples in the hanging wall of the RED, cooling from high-grade metamorphism (ca. 850 °C) at 1050–1030 Ma was protracted and slow, on the order of 3 °C/Myr. Samples from the footwall, on the other hand, appear to have been at (U)HT conditions until just before cooling through the closure temperature of Ar in amphibole (see Blereau et al., in press; Drüppel et al., 2013). A conservative estimate of peak T of 850 °C at 950 Ma implies a cooling rate of 25–30 °C/Myr in the footwall, which requires tectonically driven exhumation (Fig. 11B; Scibiorski et al., 2015). Cooling through the closure temperature of Ar in biotite (taken here as 350 °C) took on average 45 Myr, corresponding to a slow cooling rate of ca. 4 °C/Myr, consistent with slow, post-orogenic cooling of the foot- and hanging wall together during erosional exhumation (e.g., Scibiorski et al., 2015).

The thermal model and cooling rates also provide a means to constrain the amount of displacement along the RED. Although the timing of peak temperature in the footwall is difficult to constrain, a compilation of U–Pb data suggests a peak at ca. 1000 Ma (Drüppel et al., 2013; Slagstad et al., 2018), at a temperature of ca. 900 °C (Blereau et al., 2017; Drüppel et al., 2013) corresponding to a depth of 27 km (7 kbar) in our temperature model. Based on the long-lived nature of high-grade metamorphism in the SW SNO, we infer that these PT conditions remained essentially unchanged until extension started at 980 Ma. Temperatures in the hanging wall have been estimated by assuming peak T of 850 °C at 1040 Ma, followed by slow cooling of 3 °C/Myr, which yields a temperature of 670 °C at 980 Ma, corresponding to a depth of 19 km (5 kbar) in our temperature model. These estimates suggest 8 km of vertical displacement (19 km of dip-slip displacement at an average dip of 25°) along the extensional detachments, amounting to a pre-extensional temperature gradient of ca. 29 °C/km in the mid-crust.

5.3. Implications for the thermal evolution of the deep crust in the SNO

Extensional detachments are widely recognized as important components in extending the crustal pile in the later stages of orogenesis (Andersen, 1998; Jackson, 1987; Platt and Vissers, 1989; Tirel et al., 2008; Wernicke, 1981). These low-angle shear zones can rapidly exhume high-grade rocks from depth and juxtapose crustal blocks showing different tectonic and metamorphic evolution (Campani et al., 2010; Platt et al., 2015). Lithospheric delamination (Harris et al., 2002; Wells and Hoisch, 2008) or orogenic collapse (Osmundsen et al., 2006; Viola et al., 2011) are often cited as major driving forces for the formation of such major crustal thinning structures. The formation of metamorphic core complexes (Armstrong, 1982; Lister and Davis, 1989), where opposing senses of shear on coupled extensional shear zones exhume lower crust in whale-back geometries (Harris et al., 2002), appear to be an intrinsic part of this tectonic style (Holm et al., 1994; Osmundsen et al., 2006). In addition, such extensional detachments commonly display constrictional folding patterns where the detachment surfaces are folded into tight to isoclinal folds with fold axes parallel to the downdip transport direction (Braathen et al., 2004; Osmundsen et al., 2006). Extensional detachments have been widely recognized to be an intrinsic part of orogenic denudation in orogenic belts throughout geologic time (Aoya et al., 2005; Armstrong, 1982; Coney and Harms, 1984; Holm et al., 1994).

Previous evidence for extensional ductile tectonics is limited to the eastern parts of the SNO (Mulch et al., 2005; Scheiber et al., 2015; Viola et al., 2011), characterized by pre-extensional thrusting, crustal thickening and high-pressure metamorphism, in contrast to the SW SNO where geologic evidence suggests the crust remained thin. In the newly discovered RED, we observe top-to-NE orthogonal extensional ductile displacement with the development of tight to isoclinal folds in the shear zone representing a constrictional geometry that is typical of major extensional detachments in the crust (Holm et al., 1994; Platt and Vissers, 1989). Whether the combination of juxtaposed metamorphic grades and the presence of crustal-scale extensional structures in this case represent a metamorphic core complex is still enigmatic since a kinematically opposing set of detachments is not observed south and west of the RAP as it is unexposed in the North Sea.

As discussed by Slagstad et al. (2020), the duration of extension and localization in both thick and thin orogenic crust as well as in the orogenic foreland point to an external driving force, such a slab rollback,

rather than gravitationally driven 'collapse'. Slab rollback has previously been inferred to drive mafic underplating and lower-crustal melting well after the peak of orogenic activity (defined here as the end of widespread contractional deformation) at ca. 1000 Ma (Granseth et al., 2020) and several other lines of evidence suggest that the deep crust of the SNO remained hot well after the main orogenic event. A 920 Ma granitic dike in the hanging wall to the RED cuts leucosomes and high-grade metamorphic fabrics dated at 1039 Ma, suggesting that partial melting was still taking place at depth in the crust. This is perhaps unsurprising considering that emplacement of the BKSK a few tens of kilometers farther south took place between 930 and 916 Ma (Vander Auwera et al., 2011). However, emplacement of the granites until 930 Ma (Granseth et al., 2020) and pegmatites as young as 901 Ma in the central SNO (Müller et al., 2017), show that the deep crust was producing melt well after the main orogenic event. In the central SNO, isotopic data are consistent with continuous addition of juvenile material, and east in the SNO, in the Idefjorden lithotectonic unit, emplacement of the Hakefjorden norite-anorthosite complex at 916 Ma (Scherstén et al., 2000) suggests that upwelling of mantle-derived basaltic melts (see Årebäck and Stigh, 1997 for petrogenetic interpretation) continued throughout the orogen well after the main tectonic activity had ceased. Along with 970–960 Ma anorthosite in the Caledonian Jotun Nappe Complex, widely believed to represent the pre-Caledonian margin of Fennoscandia (Lundmark and Corfu, 2008), the available data from the SNO suggest that anorthosite was being formed throughout the duration of the orogeny. Present-day exposure is most likely related to differential exhumation, i.e., Caledonian nappe stacking for the Jotun anorthosite and extensional exhumation for the RAP. Exhumation of the Hakefjorden complex is less clear, but extension on the Mylonite Zone, separating the Idefjorden lithotectonic unit and underlying Eastern Segment, and the Porsgrunn–Kristiansand Shear Zone, separating the Bamble and Telemark lithotectonic units, until 860 Ma (Viola et al., 2011) and 880 Ma (Mulch et al., 2005), respectively, may have been important. However, the ductile extension we observe in the RED represents a deeper structural level, with more through-going structures and as such probably represents the most tectonically significant extensional detachment seen in the SNO.

5.4. Tectonic significance of Proterozoic massif-type anorthosites

In recent years, debate on the tectonic setting of the SNO has seen one camp advocating Himalayan–Tibetan-style continent–continent collision (e.g., Bingen et al., 2021; Möller et al., 2015) and another arguing for development of a wide continental back-arc coupled with accretionary tectonics behind an active margin (Granseth et al., 2021; Slagstad et al., 2020). As discussed elsewhere, a Himalayan-style collision is clearly at odds with the recorded (U)HT metamorphic conditions in the SW SNO, the duration of $>$ 100 Myr, as well as the trend towards higher grades at lower structural levels. By comparison, Himalayan–Tibetan metamorphism rarely reaches temperatures in excess of 750–800 °C, with durations up to at most 20–30 Myr, and characterized by inverted metamorphic isograds (e.g., Goscombe et al., 2018; Jamieson et al., 2004). The very hot crust of the SW SNO is unlikely to have been able to sustain significant crustal thickening, with shortening accommodated by lateral crustal flow (e.g., Vanderhaeghe and Teyssier, 2001). A similar process has been inferred for the Himalayan–Tibetan system (Clark and Royden, 2000), however, with orogen-wide extension in the SNO from ca. 980 Ma, any radiogenic heat source would have all but disappeared and unable to account for continued (U)HT metamorphism. In the case of the SW SNO, the slow cooling observed from as early as 1050–1030 Ma suggests that it may never have reached significant crustal thickness (e.g., Fossen et al., 2017), consistent with the lack of high-pressure metamorphism. Interestingly, recent attempts at explaining the SNO in terms of continent–continent collision invoke pre-collisional thickening of the crust followed by thinning (not thickening) at the onset of purported collision at 1050 Ma, with the crust remaining thin throughout the orogenic period (Bingen et al., 2021). The obvious problems with this model have been discussed elsewhere (Slagstad et al., 2020), suffice it to say that it shares few, if any, similarities to the evolution of the Himalayan–Tibetan system, characterized by crustal thickening at the onset of collision, sustained by continued convergence between India and Asia.

Despite decades of work on Proterozoic massif-type anorthosite around the world, no consensus has been reached as to their source, emplacement mechanism, tectonic setting, and temporal restriction (2.6–0.5 Ga; Ashwal and Bybee, 2017). The most widely accepted petrogenetic model invokes ponding and fractionation of mantle-derived basaltic melts near the Moho that produced large volumes of low-density, plagioclase-rich flotation cumulates along with dense, mafic cumulates (Ashwal, 1993; Ashwal and Bybee, 2017). An alternative scenario, developed mainly by work on the RAP, poses that subduction and melting of lower-crustal tongues provided the anorthositic parental melts (Duchesne et al., 1999). Proposed emplacement mechanisms range from buoyancy-driven diapirism to conduit ascent, and while some workers have argued that diapirism is implausible (Royse and Park, 2000), others have provided structural and finite element modeling data arguing for its feasibility, including for the RAP (Barnichon et al., 1999; Duchesne et al., 1985). Most tectonic settings have been proposed for anorthosite formation at one time or another, but in recent years consensus has shifted towards convergent margin settings, either related to late-to post-collisional delamination events that provide short-lived influx of asthenosphere-derived basaltic magma (e.g., Corrigan and Hanmer, 1997) or longer-lived Andean-type margins (Bybee et al., 2014; Bybee et al., 2019; Lehmann et al., 2020). An important recent development is the recognition that massif-type anorthosites were emplaced over long periods of time, in some cases up to or exceeding 100 Myr (Bybee et al., 2014; Bybee et al., 2019; Lehmann et al., 2020; Myers et al., 2008). This provides important constraints on both petrogenesis and tectonic setting, and also opens for the possibility that anorthosite formation and final emplacement may occur in different settings (Ashwal and Bybee, 2017).

Geochronologic data from the RAP, discussed above, suggest that its oldest known component, the Egersund–Ogna anorthosite lobe, started forming at ca. 1040 Ma, coeval with voluminous granitic magmatism and high-grade metamorphism in a regional compressional setting. There is no evidence for significant crustal thickening in the SW and central SNO, thus the only viable heat source is from underplating of mantle-derived mafic magmas. Sm–Nd isotopic data from the coeval granites and anorthosites (Bybee et al., 2014; Granseth et al., 2020) show that the anorthosites are significantly more juvenile than the granites, thus requiring mantle-derived basaltic magmas not only as a source of heat but also material to anorthosite formation. The available data from the SW SNO therefore clearly point to ponding of mantle-derived basaltic magma as the source of the anorthosite (see also Bybee et al., 2014). This realization also has significant implications for the cause of regional compression. Slagstad et al. (2013) suggested that east-dipping flat-slab subduction west of the SNO might have resulted in compression; however, the crust in the central and SW SNO was thin, hot and weak at this time and most likely incapable of transmitting significant stress to the eastern parts of the orogen that experienced coeval high-pressure metamorphism (Söderlund et al., 2008). A more likely scenario is, therefore, that accretionary events farther inboard on the fragmented continental margin, possibly driven by convection underneath the continental back-arc (e.g., Bial et al., 2015; Hyndman, 2019) caused the compression (Slagstad et al., 2020). The onset of RAP magmatism is related to long-lived, crustally derived granitic magmatism and associated high-grade metamorphism unrelated to crustal thickening but in an overall compressive setting, thus invalidating tectonic scenarios including short-lived delamination, crustal tongues, or rifting.

Compression in the SNO peaked around 1000–990 Ma and involved high-pressure metamorphism and crustal thickening east in the orogen, while the central and SW SNO crust remained relatively thin. The

ensuing extension started shortly thereafter and lasted until at least 930 Ma and involved the entire SNO and its eastern foreland. While gravitationally driven extension might have contributed in the previously thickened eastern part of the orogen, extension in central and SW parts, as well as in the foreland, require an external driving force such as slab roll-back (Slagstad et al., 2020), as indicated by higher lower-crustal temperatures interpreted to reflect increased basaltic underplating (Granseth et al., 2020). The Garsaknatt intrusion is still undated but appears to be structurally located in the southern continuation of the RED, the Farsund shear zone. Unlike the rest of the RAP, which has a distinct nested-lobe geometry ascribed to diapirism, the Garsaknatt anorthosite is elongate and most likely formed sometime during the 980–930 Ma extensional phase.

The tectonic setting of the SNO at or behind the SW active margin of Fennoscandia and the link between different orogenic stages and anorthosite formation over a period of around 100 Myr, are similar to recent interpretations of anorthosite petrogenesis in other parts of the world. Many of the Paleo- and Mesoproterozoic anorthosites in southeastern Laurentia (Grenville and Nain provinces) and the Kunene anorthosite complex in southern Africa are now ascribed to active-margin processes with durations of tens of million years up to and exceeding 100 Myr (Bybee et al., 2014; Bybee et al., 2019; Myers et al., 2008). Bybee et al. (2014) argued that the RAP and similar massif-type anorthosites formed in an arc setting. While this accounts for the apparent duration of anorthosite formation and associated metamorphic and magmatic processes, the dry basaltic magmas needed to stabilize large volumes of cumulate plagioclase appear incompatible with formation in the arc itself. A more likely scenario, based on the duration, conditions, and compositions of metamorphism and magmatism, as well as the structural evolution delineated here, is formation in a continental back-arc setting, as suggested by Slagstad et al. (2020) for the SNO and discussed more generally by Collins et al. (2021).

Although the RAP has been extensively studied, we now know that many of the previous models were based on erroneous assumptions, in particular the short duration (2–3 Myr) and anorogenic "character" (Schärer et al., 1996), but also the presence of a regional orthopyroxene-in isograd that was supposed to account for dry lower-crustal conditions (Vander Auwera et al., 2011), and melting of crustal tongues (Duchesne et al., 1999). Rather, the RAP appears to have formed over a period of about 100 Myr during long-lived compression and extension, both operating on time scales of many tens of million years, behind an active continental margin with a distribution of metamorphic rocks (isograds) that is largely related to late-stage differential exhumation. It seems likely that many of the controversies and disagreements regarding anorthosite petrogenesis will become smaller as more geochronological data is collected from these rocks and their relationship to and history of their host orogens are better understood.

6. Conclusions

The main outcomes of this study are:

(1) The exposed rocks in the SW SNO do not constitute a horizontal slice through orogenic crust, but structural juxtaposition of different crustal levels along ca. 980–930 Ma extensional ductile detachments, collectively referred to as the Rogaland Extensional Detachment (RED).
(2) The RED forms an array of NW–SE-striking, E–NE gently dipping, ductile shear zones with a presently mapped minimum 40 km strike length in an anastomosing zone at least 15 km wide. These shear zones are not typically mylonitic but display high-temperature asymmetries such as sigma clasts, delta clasts, asymmetric boudinage, extensional shear bands, and a weak E–NE stretching lineation, recording a top-to-E or NE extensional dip-slip to oblique displacement from ca. 980 to 930 Ma. The RED is folded on regional scale constrictional folds with NE-plunging tight to isoclinal folds, parallel to the transport direction.
(3) The RED represents the first identified major crustal-scale detachment within the western part of the orogen and arguably the largest extensional structure in the whole SNO. Thermal modeling suggests approximately 8 km of vertical displacement, with approximately 19 km of horizontal displacement.
(4) The steep brittle extensional structures in the hanging wall to the RED, which host numerous small Mo deposits, display similar kinematics to the regional-scale crustal extension and reflect the disintegration of the hanging wall during exhumation through the brittle–ductile transition; thus we suggest that the distribution of the mineral deposit is closely linked to the evolution of the large-scale tectonic structures.
(5) The weight of geochronological data, cooling history, and field constraints suggest that the RAP was emplaced well before the generally accepted age of 930 Ma, most likely $>$ 950 Ma. Emplacement was probably polybaric, consistent with petrologic data, and long-lived (on the order of 100 Myr).
(6) Early anorthosite emplacement was by diapirism, inhibited or facilitated by changing compressional and extensional regional stress fields, respectively, whereas later anorthositic magmas may have migrated along active extensional detachments.
(7) The lower SNO crust remained hot until ca. 915–900 Ma, i.e., well after termination of orogenic activity recorded at higher crustal levels, and capable of producing melt.

Declaration of Competing Interest

The authors declare that they have no known competing financial interests or personal relationships that could have appeared to influence the work reported in this paper.

Acknowledgements

Journal reviewers Grant Bybee and Bill Collins are thanked for insightful and critical comments that helped to improve the manuscript significantly. Wilson Teixeira is thanked for editorial handling. Yanbo Cheng is thanked for preparing samples for Re–Os dating and Olivier Bolle for discussions on anorthosite emplacement. We would also like to thank the Geological Survey of Norway (NGU), British Geological Survey (BGS), University of Bergen (UiB), and University of Alberta (U of A) for access to lab facilities. EVK thanks the Research Council of Norway (RCN) for support through its Centers of Excellence funding scheme (project 223272: CEED). This work forms part of the NGU project 390600: Tectonic Setting of Wolfram and Molybdenite deposits in southern Norway in the Mineral Resources Division.

Appendix A. Supplementary data

Supplementary data associated with this article can be found, in the online version, at https://doi.org/10.1016/j.precamres.2022.106695.

References

Afonso, J.C., Ranalli, G., 2004. Crustal and mantle strengths in continental lithosphere: Is the jelly sandwich model obsolete? Tectonophysics 394 (3-4), 221–232.
Andersen, T., Griffin, W.L., 2004. Lu-Hf and U-Pb isotope systematics of zircons from the Storgangen intrusion, Rogaland Intrusive Complex, SW Norway: Implications for the composition and evolution of Precambrian lower crust in the Baltic Shield. Lithos 73 (3-4), 271–288.
Andersen, T.B., 1998. Extensional tectonics in the Caledonides of southern Norway, an overview. Tectonophysics 285 (3-4), 333–351.
Andersson, M., Lie, J.E., Husebye, E.S., 1996. Tectonic setting of post-orogenic granites within SW Fennoscandia based on deep seismic and gravity data. Terra Nova 8 (6), 558–566.
Aoya, M., Wallis, S.R., Terada, K., Lee, J., Kawakami, T., Wang, Y.u., Heizler, M., 2005. North-south extension in the Tibetan crust triggered by granite emplacement. Geology 33 (11), 853. https://doi.org/10.1130/G21806.110.1130/2005169.

Årebäck, H., Stigh, J., 1997. Polybaric evolution of the Hakefjorden Complex, southwestern Sweden, deduced from partial dissolution in andesine megacrysts. Geol. Foeren. Stockholm Foerh. 119 (2), 97–101.
Armstrong, R.L., 1982. Cordilleran Metamorphic Core Complexes – From Arizona to Southern Canada. Annu. Rev. Earth Planet. Sci. 10 (1), 129–154.
Ashwal, L.D., 1993. Anorthosites. Springer-Verlag, Berlin.
Ashwal, L.D., Bybee, G.M., 2017. Crustal evolution and the temporality of anorthosites. Earth Sci. Rev. 173, 307–330.
Barnichon, J.D., Havenith, H., Hoffer, B., Charlier, R., Jongmans, D., Duchesne, J.C., 1999. The deformation of the Egersund-Ogna anorthosite massif, south Norway: finite-element modelling of diapirism. Tectonophysics 303 (1-4), 109–130.
Bial, J., Büttner, S.H., Schenk, V., Appel, P., 2015. The long-term high-temperature history of the central Namaqua Metamorphic Complex: Evidence for a Mesoproterozoic continental back-arc in southern Africa. Precambr. Res. 268, 243–278.
Bingen, B., Boven, A., Punzalan, L., Wijbrans, J.R., Demaiffe, D., 1998. Hornblende $^{40}Ar/^{39}Ar$ geochronology across terrane boundaries in the Sveconorwegian Province of S. Norway. Precambrian Research 90 (3-4), 159–185.
Bingen, B., Davis, W.J., Hamilton, M.A., Engvik, A.K., Stein, H.J., Skår, Ø., Nordgulen, Ø., 2008a. Geochronology of high-grade metamorphism in the Sveconorwegian belt, S. Norway: U-Pb, Th-Pb and Re-Os data. Norw. J. Geol. 88, 13–42.
Bingen, B., Nordgulen, Ø., Viola, G., 2008b. A four-phase model for the Sveconorwegian orogeny, SW Scandinavia. Norw. J. Geol. 88, 43–72.
Bingen, B., Stein, H., 2003. Molybdenite Re-Os dating of biotite dehydration melting in the Rogaland high-temperature granulites, S Norway. Earth Planet. Sci. Lett. 208 (3-4), 181–195.
Bingen, B., Viola, G., Möller, C., Vander Auwera, J., Laurent, A., Yi, K., 2021. The Sveconorwegian orogeny. Gondwana Res. 90, 273–313.
Blereau, E., Clark, C., Jourdan, F., Johnson, T.E., Taylor, R.J.M., Kinny, P.D., Danišík, M., Hand, M., Eroglu, E., 2019. Closed system behaviour of argon in osumilite records protracted high-T metamorphism within the Rogaland-Vest Agder Sector, Norway. J. Metamorph. Geol. 37 (5), 667–680.
Blereau, E., Clark, C., Kinny, P.D., Sansom, E., Taylor, R.J.M., Hand, M., in press. Probing the history of UHT metamorphism through rare earth element diffusion in zircon. Journal of Metamorphic Geology n/a.
Blereau, E., Johnson, T.E., Clark, C., Taylor, R.J.M., Kinny, P.D., Hand, M., 2017. Reappraising the P-T evolution of the Rogaland-Vest Agder Sector, southwestern Norway. Geosci. Front. 8 (1), 1–14.
Bolle, O., Diot, H., Liégeois, J.-P., Vander Auwera, J., 2010. The Farsund intrusion (SW Norway): A marker of late-Sveconorwegian (Grenvillian) tectonism emplaced along a newly defined major shear zone. J. Struct. Geol. 32 (10), 1500–1518.
Braathen, A., Osmundsen, P.T., Gabrielsen, R.H., 2004. Dynamic development of fault rocks in a crustal-scale detachment: An example from. Tectonics 23 (4), n/a–n/a.
Brewer, T.S., Åhäll, K.-I., Menuge, J.F., Storey, C.D., Parrish, R.R., 2004. Mesoproterozoic bimodal volcanism in SW Norway, evidence for recurring pre-Sveconorwegian continental margin tectonism. Precambr. Res. 134 (3-4), 249–273.
Bybee, G.M., Ashwal, L.D., Shirey, S.B., Horan, M., Mock, T., Andersen, T.B., 2014. Pyroxene megacrysts in Proterozoic anorthosites: Implications for tectonic setting, magma source and magmatic processes at the Moho. Earth Planet. Sci. Lett. 389, 74–85.
Bybee, G.M., Hayes, B., Owen-Smith, T.M., Lehmann, J., Ashwal, L.D., Brower, A.M., Hill, C.M., Corfu, F., Manga, M., 2019. Proterozoic massif-type anorthosites as the archetypes of long-lived (≥100 Myr) magmatic systems—New evidence from the Kunene Anorthosite Complex (Angola). Precambr. Res. 332, 105393. https://doi.org/10.1016/j.precamres.2019.105393.
Campani, M., Mancktelow, N., Seward, D., Rolland, Y., Müller, W., Guerra, I., 2010. Geochronological evidence for continuous exhumation through the ductile-brittle transition along a crustal-scale low-angle normal fault: Simplon Fault Zone, central Alps. Tectonics 29 (3). https://doi.org/10.1029/2009TC002582.
Charlier, B., Duchesne, J.-C., Vander Auwera, J., Storme, J.-Y., Maquil, R., Longhi, J., 2010. Polybaric fractional crystallization of high-alumina basalt parental magmas in the Egersund-Ogna massif-type anorthosite (Rogaland, SW Norway) constrained by plagioclase and high-alumina orthopyroxene megacrysts. J. Petrol. 51 (12), 2515–2546.
Clark, C., Fitzsimons, I.C.W., Healy, D., Harley, S.L., 2011. How does the continental crust get really hot? Episodes 7 (4), 235–240.
Clark, M.K., Royden, L.H., 2000. Topographic ooze: Building the eastern margin of Tibet by lower crustal flow. Geology 28, 703–706.
Clauser, C., Huenges, E., 1995. Thermal conductivity of rocks and minerals, Rock Physics and Phase Relations. A Handbook of Physical Constants. AGU Reference Shelf 3, 105–126.
Coint, N., Slagstad, T., Roberts, N.M.W., Marker, M., Røhr, T., Sørensen, B.E., 2015. The Late Mesoproterozoic Sirdal Magmatic Belt, SW Norway: Relationships between magmatism and metamorphism and implications for Sveconorwegian orogenesis. Precambr. Res. 265, 57–77.
Collins, W.J., Murphy, J.B., Blereau, E., Huang, H.-Q., 2021. Water availability controls crustal melting temperatures. Lithos 402-403, 106351. https://doi.org/10.1016/j.lithos.2021.106351.
Coney, P.J., Harms, T.A., 1984. Cordilleran metamorphic core complexes: Cenozoic extensional relics of Mesozoic compression. Geology 12 (9), 550. https://doi.org/10.1130/0091-7613(1984)12<550:CMCCCE>2.0.CO;2.
Corfu, F., 2019. The Sognefjell volcanic-subvolcanic complex – A late Sveconorwegian arc imbricated in the central Norwegian Caledonides. Precambr. Res. 331, 105353. https://doi.org/10.1016/j.precamres.2019.105353.
Corrigan, D., Hanmer, S., 1997. Anorthosites and related granitoids in the Grenville orogen: A product of convective thinning of the lithosphere? Geology 25 (1), 61. https://doi.org/10.1130/0091-7613(1997)025<0061:AARGIT>2.3.CO;2.
Druppel, K., Elsasser, L., Brandt, S., Gerdes, A., 2013. Sveconorwegian mid-crustal ultrahigh-temperature metamorphism in Rogaland, Norway: U-Pb LA-ICP-MS geochronology and pseudosections of sapphirine granulites and associated paragneisses. J. Petrol. 54 (2), 305–350.
Duchesne, J.-C., 2001. The Rogaland Intrusive Massifs - an excursion guide. NGU Report 139.
Duchesne, J.C., Liegeois, J.P., Vander Auwera, J., Longhi, J., 1999. The crustal tongue melting model and the origin of massive anorthosites. Terra Nova 11 (2-3), 100–105.
Duchesne, J.C., Maquil, R., Demaiffe, D., 1985. The Rogaland anorthosites; facts and speculations, in: Tobi, A.C.e., Touret, J.L.R. (Eds.), deep Proterozoic crust in the North Atlantic provinces. D. Reidel Publishing Company, Dordrecht-Boston, International. ISSN: 0377-2071, p. 449.
Falkum, T., 1982. Geologisk kart over Norge, berggrunnskart MANDAL, 1:250,000. Norges geologiske undersøkelse.
Fossen, H., Cavalcante, G.C., de Almeida, R.P., 2017. Hot Versus Cold Orogenic Behavior: Comparing the Araçuaí-West Congo and the Caledonian Orogens. Tectonics 36 (10), 2159–2178.
Goscombe, B., Gray, D., Foster, D.A., 2018. Metamorphic response to collision in the Central Himalayan Orogen. Gondwana Res. 57, 191–265.
Granseth, A., Slagstad, T., Coint, N., Roberts, N.M.W., Røhr, T.S., Sørensen, B.E., 2020. Tectonomagmatic evolution of the Sveconorwegian orogen recorded in the chemical and isotopic compositions of 1070–920 Ma granitoids. Precambr. Res. 340, 105527. https://doi.org/10.1016/j.precamres.2019.105527.
Granseth, A., Slagstad, T., Roberts, N.M.W., Hagen-Peter, G., Kirkland, C.L., Møkkelgjerd, S.H.H., Røhr, T.S., Coint, N., Sørensen, B.E., 2021. Multi-isotope tracing of the 1.3–0.9 Ga evolution of Fennoscandia; crustal growth during the Sveconorwegian orogeny. Gondwana Res. 91, 31–39.
Harris, L.B., Koyi, H.A., Fossen, H., 2002. Mechanisms for folding of high-grade rocks in extensional tectonic settings. Earth Sci. Rev. 59 (1-4), 163–210.
Holm, D.K., Fleck, R.J., Lux, D.R., 1994. The Death Valley turtlebacks reinterpreted as Miocene- Pliocene folds of a major detachment surface. J. Geol. 102 (6), 718–727.
Hyndman, R.D., 2019. Mountain building orogeny in precollision hot backarcs: North American Cordillera, India-Tibet, and Grenville Province. J. Geophys. Res. Solid Earth 124, 2057–2079.
Jackson, J.A., 1987. Active normal faulting and crustal extension, in: Coward, M.P., Dewey, J.F., Hancock, P.L. (Eds.), Continental extensional tectonics, pp. 3-18.
Jamieson, R.A., Beaumont, C., Medvedev, S., Nguyen, M.H., 2004. Crustal channel flows: 2. Numerical models with implications for metamorphism in the Himalayan-Tibetan orogen. Journal of Geophysical Research 109, B06407, doi:06410.01029/02003JB002811.
Jaupart, C., Mareschal, J.C., 1999. The thermal structure and thickness of continental roots. Lithos 48, 93–114.
Karykowski, B.T., Maier, W.D., 2017. Microtextural characterisation of the Lower Zone in the western limb of the Bushveld Complex, South Africa: evidence for extensive melt migration within a sill complex. Contrib. Miner. Petrol. 172, 60.
Latypov, R., Chistyakova, S., 2022. Misinterpretation of zircon ages in layered intrusions. S. Afr. J. Geol. 125 (1), 13–26.
Laurent, A.T., Bingen, B., Duchene, S., Whitehouse, M.J., Seydoux-Guillaume, A.-M., Bosse, V., 2018. Decoding a protracted zircon geochronological record in ultrahigh temperature granulite, and persistence of partial melting in the crust, Rogaland. Norway. Contributions to Mineralogy and Petrology 173, 29.
Lehmann, J., Bybee, G.M., Hayes, B., Owen-Smith, T.M., Belyanin, G., 2020. Emplacement of the giant Kunene AMCG complex into a contractional ductile shear zone and implications for the Mesoproterozoic tectonic evolution of SW Angola. Int. J. Earth Sci. 109 (4), 1463–1485.
Lewerentz, A., Harlov, D.E., Scherstén, A., Whitehouse, M.J., 2019. Baddeleyite formation in zircon by Ca-bearing fluids in silica-saturated systems in nature and experiment: resetting of the U-Pb geochronometer. Contrib. Miner. Petrol. 174, 64.
Lister, G.S., Davis, G.A., 1989. The origin of metamorphic core complexes and detachment faults formed during Tertiary continental extension in the northern Colorado River region, U.S.A. J. Struct. Geol. 11 (1-2), 65–94.
Longhi, J., Fram, M.S., Vander Auwera, J., Montieth, J.N., 1993. Pressure effects, kinetics, and rheology of anorthositic and related magmas. Am. Mineral. 78, 1016–1030.
Lundmark, A.M., Corfu, F., 2008. Late-orogenic Sveconorwegian massif anorthosite in the Jotun Nappe Complex, SW Norway, and causes of repeated AMCG magmatism along the Baltoscandian margin. Contrib. Miner. Petrol. 155 (2), 147–163.
Maquil, R., Duchesne, J.C., 1984. Geothermometrie par les pyroxene et mise en place du massif anorthositique d'Egersund-Ogna (Rogaland, Norvege meridionale). Annales de la Société Géologique de Belgique 107, 27–49.
Marker, M., Schiellerup, H., Meyer, G.B., Robins, B., Bolle, O., 2003. An introduction to the geological map of the Rogaland Anorthosite Province 1:75,000. In: Duchesne, J. C., Korneliussen, A. (Eds.), Ilmenite deposits and their geological environment. NGU, Trondheim, pp. 109–116.
Maystrenko, Y., Olesen, O., Ebbing, J., Nasuti, A., 2017. Deep structure of the northern North Sea and south-western Norway based on 3D density and magnetic modelling. Norw. J. Geol. 97, 169–210.
Möller, C., Andersson, J., Dyck, B., Antal Lundin, I., 2015. Exhumation of an eclogite terrane as a hot migmatitic nappe, Sveconorwegian orogen. Lithos 226, 147–168.
Mukherjee, A.B., Das, S., Sen, D., Bhattacharya, B., 2020. Buoyant rise of anorthosite from a layered basic complex triggered by Rayleigh-Taylor instability: Insights from a numerical modeling study. Am. Mineral. 105, 437–446.

Mulch, A., Cosca, M., Andresen, A., Fiebig, J., 2005. Time scales of deformation and exhumation in extensional detachment systems determined by high-spatial resolution in situ UV-laser 40Ar/39Ar dating. Earth Planet. Sci. Lett. 233 (3-4), 375–390.

Müller, A., Romer, R.L., Pedersen, R.-B., 2017. The Sveconorwegian Pegmatite Province – Thousands of Pegmatites Without Parental Granites. The Canadian Mineralogist 55 (2), 283–315.

Myers, J.S., Voordouw, R.J., Tettelaar, T.A., 2008. Proterozoic anorthosite-granite Nain batholith: structure and intrusion processes in an active lithosphere-scale fault zone, northern Labrador. Can. J. Earth Sci. 45 (8), 909–934.

Osmundsen, P.T., Eide, E.A., Haabesland, N.E., Roberts, D., Andersen, T.B., Kendrick, M., Bingen, B., Braathen, A., Redfield, T.F., 2006. Kinematics of the Høybakken detachment zone and the Møre-Trøndelag Fault Complex, central Norway. Journal of the Geological Society 163 (2), 303–318.

Platt, J.P., Behr, W.M., Cooper, F.J., 2015. Metamorphic core complexes: windows into the mechanics and rheology of the crust. Journal of the Geological Society 172 (1), 9–27.

Platt, J.P., Vissers, R.L.M., 1989. Extensional collapse of thickened continental lithosphere: A working hypothesis for the Alboran Sea and Gibraltar arc. Geology 17 (6), 540. https://doi.org/10.1130/0091-7613(1989)017<0540:ECOTCL>2.3.CO;2.

Robins, B., Tumyr, O., Tysseland, M., Garmann, L.B., 1997. The Bjerkreim-Sokndal Layered Intrusion, Rogaland, SW Norway: Evidence from marginal rocks for a jotunite parent magma. Lithos 39, 121–133.

Royse, K.R., Park, R.G., 2000. Emplacement of the Nain anorthosite: diapiric versus conduit ascent. Can. J. Earth Sci. 37 (8), 1195–1207.

Schärer, U., Wilmart, E., Duchesne, J.-C., 1996. The short duration and anorogenic character of anorthosite magmatism: U-Pb dating of the Rogaland complex, Norway. Earth Planet. Sci. Lett. 139 (3-4), 335–350.

Scheiber, T., Viola, G., Bingen, B., Peters, M., Solli, A., 2015. Multiple reactivation and strain localization along a Proterozoic orogen-scale deformation zone: The Kongsberg-Telemark boundary in southern Norway revisited. Precambr. Res. 265, 78–103.

Scherstén, A., Årebäck, H., Cornell, D., Hoskin, P., Åberg, A., Armstrong, R., 2000. Dating mafic–ultramafic intrusions by ion-microprobing contact-melt zircon: examples from SW Sweden. Contrib. Miner. Petrol. 139 (1), 115–125.

Schiellerup, H., 2001. Igneous processes in anorthosites and ilmenite-bearing plutons in the Rogaland Anorthosite Province. Norwegian University of Science and Technology, Trondheim, Southwest Norway.

Scibiorski, E., Tohver, E., Jourdan, F., 2015. Rapid cooling and exhumation in the western part of the Mesoproterozoic Albany-Fraser Orogen, Western Australia. Precambr. Res. 265, 232–248.

Sigmond, E.M.O., 1978. Beskrivelse til det berggrunnsgeologiske kartbladet Sauda 1: 250,000. Nor. Geol. Unders. 341, 1–94.

Slagstad, T., 2006. Did hot, high heat-producing granites determine the location of the Oslo Rift? Tectonophysics 412 (1-2), 105–119.

Slagstad, T., 2008. Radiogenic heat production of Archaean to Permian geological provinces in Norway. Norw. J. Geol. 88, 149–166.

Slagstad, T., Balling, N., Elvebakk, H., Midttømme, K., Olesen, O., Olsen, L., Pascal, C., 2009. Heat-flow measurements in Late Palaeoproterozoic to Permian geological provinces in south and central Norway and a new heat-flow map of Fennoscandia and the Norwegian - Greenland Sea. Tectonophysics 473 (3-4), 341–361.

Slagstad, T., Marker, M., Roberts, N.M.W., Saalmann, K., Kirkland, C.L., Kulakov, E., Ganerød, M., Røhr, T.S., Møkkelgjerd, S.H.H., Granseth, A., Sørensen, B.E., 2020. The Sveconorwegian orogeny – Reamalgamation of the fragmented southwestern margin of Fennoscandia. Precambr. Res. 350, 105877. https://doi.org/10.1016/j.precamres.2020.105877.

Slagstad, T., Roberts, N.M.W., Coint, N., Høy, I., Sauer, S., Kirkland, C.L., Marker, M., Røhr, T.S., Henderson, I.H.C., Stormoen, M.A., Skår, Ø., Sørensen, B.E., Bybee, G.M., 2018. Magma-driven, high-grade metamorphism in the Sveconorwegian Province, SW Norway during the terminal stages of Fennoscandian Shield evolution. Geosphere 14, 861–882.

Slagstad, T., Roberts, N.M.W., Marker, M., Røhr, T.S., Schiellerup, H., 2013. A non-collisional, accretionary Sveconorwegian orogen. Terra Nova 25 (1), 30–37.

Smithson, S.B., Ramberg, I.B., 1979. Gravity interpretation of the Egersund anorthosite complex, Norway: Its petrological and geothermal significance. GSA Bulletin 90 (2), 199. https://doi.org/10.1130/0016-7606(1979)90<199:GIOTEA>2.0.CO;2.

Söderlund, U., Hellström, F.A., Kamo, S.L., 2008. Geochronology of high-pressure mafic granulite dykes in SW Sweden: tracking the P-T–t path of metamorphism using Hf isotopes in zircon and baddeleyite. J. Metamorph. Geol. 26 (5), 539–560.

Söderlund, U., Isachsen, C.E., Bylund, G., Heaman, L.M., Jonathan Patchett, P., Vervoort, J.D., Andersson, U.B., 2005. U-Pb baddeleyite ages and Hf, Nd isotope chemistry constraining repeated mafic magmatism in the Fennoscandian Shield from 1.6 to 0.9 Ga. Contrib. Miner. Petrol. 150 (2), 174–194.

Spencer, C.J., Roberts, N.M.W., Cawood, P.A., Hawkesworth, C.J., Prave, A.R., Antonini, A.S.M., Horstwood, M.S.A., 2014. Intermontane basins and bimodal volcanism at the onset of the Sveconorwegian Orogeny, southern Norway. Precambr. Res. 252, 107–118.

Stormoen, M.A., 2015. Synkinematic intrusion of granitoid sheets, with implications for molybdenite deposits in the Knaben Zone, Sirdal Magmatic Belt, SW Norway. In: Department of Geology and Mineral Resources Engineering. Norwegian University of Science and Technology, Trondheim, p. 131.

Tirel, C., Brun, J.-P., Burov, E., 2008. Dynamics and structural development of metamorphic core complexes. Journal of Geophysical Research: Solid. Earth 113 (B4). https://doi.org/10.1029/2005JB003694.

Tobi, A.C., Hermanns, G.A.E.M., Maijer, C., Jansen, J.B.H., 1985. Metamorphic zoning in the high-grade Proterozoic of Rogaland-Vest Agder, SW Norway. In: Tobi, A.C., Touret, J.L.R. (Eds.), The Deep Proterozoic Crust in the North Atlantic Provinces. Reidel, Dordrecht, pp. 477–497.

Tomkins, H.S., Williams, I.S., Ellis, D.J., 2005. In situ U-Pb dating of zircon formed from retrograde garnet breakdown during decompression in Rogaland, SW Norway. J. Metamorph. Geol. 23 (4), 201–215.

Vander Auwera, J., Bolle, O., Bingen, B., Liégeois, J.-P., Bogaerts, M., Duchesne, J.C., De Waele, B., Longhi, J., 2011. Sveconorwegian massif-type anorthosites and related granitoids result from post-collisional melting of a continental arc root. Earth-Sci. Rev. 107 (3-4), 375–397.

Vanderhaeghe, O., Teyssier, C., 2001. Partial melting and flow of orogens. Tectonophysics 342 (3-4), 451–472.

Viola, G., Henderson, I.H.C., Bingen, B., Hendriks, B.W.H., 2011. The Grenvillian-Sveconorwegian orogeny in Fennoscandia: Back-thrusting and extensional shearing along the "Mylonite Zone". Precambr. Res. 189 (3-4), 368–388.

Wells, M.L., Hoisch, T.D., 2008. The role of mantle delamination in widespread Late Cretaceous extension and magmatism in the Cordilleran orogen, western United States. GSA Bulletin 120 (5-6), 515–530.

Wernicke, B., 1981. Low-angle normal faults in the Basin and Range Province: nappe tectonics in an extending orogen. Nature 291 (5817), 645–648.

Westphal, M., Schumacher, J.C., Boschert, S., 2003. High-temperature metamorphism and the role of magmatic heat sources at the Rogaland Anorthosite Complex in southwestern Norway. J. Petrol. 44, 1145–1162.

Wohlgemuth-Ueberwasser, C.C., Schuessler, J.A., von Blanckenburg, F., Möller, A., 2018. Matrix dependency of baddeleyite U-Pb geochronology by femtosecond-LA-ICP-MS and comparison with nanosecond-LA-ICP-MS. J. Anal. At. Spectrom. 33 (6), 967–974.

Zoth, G., Hänel, R., 1988. Appendix. In: Hänel, R., Rybach, L., Stegena, L. (Eds.), Handbook of Terrestrial Heat Flow Density Determination. Kluwer, Dordrecht, pp. 449–466.